CONF-78-123-E
FERMILAB-CONF-78-123-E
UCD-PPL-7871
E-931

XIX. International Conference on High Energy Physics

Session A3E

Charged and Neutral Particle Production from 400 GeV/c pp Collisions

R.D. Kass, W. Ko, R.L. Lander, W. Michael,

D.E. Pellett, and P.M. Yager

University of California, Davis,

Davis, California 95616, USA

and

R. Ely and G. Gidal

Lawrence Berkeley Laboratory

Berkeley, California 94720, USA

I Introduction

A great deal of work has been done on the inclusive reactions of particle production at high energies.[1] These data include charged particle production (mostly bubble chamber results) or neutral particle production, but seldom both. Several theoretical models of particle production survived comparison to those data. To distinguish these models, one needs the simultaneous measurement of charged and neutral particles. Any study of the production of resonances that decay into charged and neutral particles also requires such data. A large hydrogen bubble chamber is well-suited to such a study due to the visibility of the production vertex and the large volume for neutral particle conversion or decay.

In this paper we present results on charged and neutral particle production from 400 GeV/c pp collisions in the Fermilab 15 foot bubble chamber. The emphasis of this work is on the inclusive and semi-inclusive production of π^o's, K^o's, Λ^o's and $\bar{\Lambda}^o$'s. Using the large number of γ's that convert to e^+e^- in the chamber liquid (5 to 10 times larger than experiments performed with the Fermilab 30 inch chamber) we are able to measure the cross section for Σ^o and $\bar{\Sigma}^o$ production. From the events with more than one converted γ's, upper limits are calculated for inclusive $\eta^o(548)$ production and, in events with fewer than 11 prongs, $\omega^o(783)$ production. Correlations between neutral and charged pions are studied in terms of $\langle\pi^o\rangle_-$ and the Mueller moments f_2^{--}, f_2^{o-}, and f_2^{oo}.

II Scanning and Measuring

The data of this experiment[2] were obtained from a 30,000 picture (6 μb/event) exposure of Fermilab's 15 foot bubble chamber to a 400 GeV/c proton beam.

Approximately 60% of the film was scanned at UC Davis and 40% at LBL. Both laboratories used SP5B scan tables equipped with dual magnification (14× and 45×) and image plane digitizers (IPD's). The IPD's were accurate to the order of 100 μm on the scan table. At LBL an IBM 7044 computer was on-line to the scan table, while at UC Davis the scan tables were controlled by a microprocessor-based system.[3]

Scanners were instructed to record all relevant characteristics of each picture, and make a judgement on its scannability. For scannable frames, quantities of interest such as number of beam tracks, charged multiplicity of an event, number of neutrals associated with an event, etc. were recorded. Events that were selected to be measured had vertex and one or two track coordinates digitized. The purpose of this digitization was to guide the measurer (at some future time) to a given track in a given view. All track matching was done by the scanner. Both the LBL and UC Davis scan systems allowed the scanner to make comments concerning a track(e.g., identity) which could later be passed on to the measurer.

Approximately 12% of the film was scanned twice in order to estimate the efficiency for locating V^o's or γ's in a single event, and to estimate the efficiency of locating events in a frame. The efficiency for locating V^o's or γ's was determined for three types of events: events with ≤ 6 prongs ($95 \pm 1.4\%$), $6 <$ prongs ≤ 12 ($90 \pm 1.5\%$) and > 12 prongs ($88 \pm 1.8\%$).

The efficiency for finding events in a frame was determined separately for two prongs (90 $\pm$ 3%) and events with > 2 prongs (99.4 $\pm$ 3%).

All events were measured with an LBL Franckenstein which utilized the CICERO[4] software/hardware package.

All event measurements were processed using TVGP and SQUAW. All tracks leaving a vertex were fitted with three different mass hypotheses (π, K, or p for a primary vertex and e, π, or p for a secondary vertex).

Tracks were rejected if the film residuals (FRMS) of the track were $\geq$ 21μm or if the track failed to reconstruct in TVGP. Tracks with large FRMS (> 21μm for all mass interpretations) comprise 3.6% of the reconstructed tracks leaving the primary vertex and 5% of the reconstructed tracks leaving the secondary vertex. For tracks leaving the primary vertex we find that 2.8% of the tracks fail to reconstruct, while for tracks coming from a secondary vertex 2.2% fail to reconstruct. The measuring efficiency for tracks from the primary vertex is 91% while the efficiency for measuring a V^o/γ is 87%.

An examination of a 15 foot bubble chamber photo reveals the fact that there are numerous poorly illuminated areas in the chamber caused by holes in the scotchlite pattern due to fiducials and the piston ring. These can obscure the location of a vertex in a view or a combination of views. It was therefore necessary to modify TVGP to find a vertex using the available measurements in this case.[2]

III Fiducial Volume

The fiducial volume for the primary vertex was chosen to be[5]:

$$-180 \leq X \leq 152 \text{ cm.}$$

Since the beam was collimated about Y = Z = 0 by the beam optics, no fiducial cut on Y or Z was necessary for primary interactions.

The fiducial volume for secondary vertices was chosen to be:

$$|X| \leq 160 \text{ cm}$$
$$|Y| \leq 160 \text{ cm}$$
$$|Z| \leq 160 \text{ cm.}$$

The wall of the chamber is located at X ≃ 190 cm, insuring that there is at least a foot in space of track for measurement. In addition, the minimum distance between the primary and secondary vertex was required to be greater than 4 (15) cm for V^o's (γ's).

IV Selection of 3c Fits

The computer program SQUAW was used to attempt a 3 constraint (3c) kinematical fit to the following reactions:

1) $\gamma p \rightarrow e^+e^- p_s$ $\qquad p_s$ = spectator proton
2) $K^o_s \rightarrow \pi^+\pi^-$
3) $\Lambda^o \rightarrow p\,\pi$
4) $\bar{\Lambda}^o \rightarrow \pi^+\,\bar{p}$.

Table 1 shows that for a sample of 3177 neutrals giving a 3c fit (confidence level > 10^{-5}) approximately 14% of the neutrals fit two or more of the above reactions. In order to assign a unique identity to these

ambiguous fits, the distribution of the transverse momentum (relative to the parent) of the negative decay product (P_T^-) was studied.

In order to resolve the V^o-γ ambiguities, an event was called a γ if P_T^- for both the V^o and γ hypotheses was $\leq$ 20 MeV/c. A small number of events (21) had P_T^- of the γ < 20 MeV/c, but P_T^- of the V^o hypothesis > 20 MeV/c (overlap in Table 1). These events were all classified as γ's. The P_T^- distribution of unique γ's is shown in Figure 1a, while the P_T^- distribution for all γ's is shown in Figure 1b. The γ sample is estimated to be at least 99% pure.

Figure 2a shows the P_T^- distribution for K^o's (reaction 2) with a unique 3c fit. This distribution peaks near the maximum value of P_T^- (206 MeV/c) but is depleted for P_T^- < 102 MeV/c, as such events may be ambiguous with the Λ^o, $\bar{\Lambda}^o$, or γ fits. The K^o's that were ambiguous with a γ were assigned to be a K^o if P_T^- of the V^o and γ were > 20 MeV/c. To separate K^o's from Λ^o's and $\bar{\Lambda}^o$'s, we require that P_T^- of the K^o be > 102 MeV/c. The K^o sample is estimated to be at least 96% pure. The P_T^- distribution of all K^o's is shown in Figure 2b. The curve in Figure 2b is what is expected from phase space normalized to the events with P_T^- > 102 MeV/c.

The P_T^- distribution for unique Λ^o fits (reaction 3) is shown in Figure 3a. This distribution is not strongly peaked at the maximum value of P_T^- (100.4 MeV/c) because most of the Λ^o's are ambiguous with γ's and K^o's. To separate the Λ^o's from the γ's, we make a cut of P_T^- > 20 MeV/c. The Λ^o-K^o ambiguity reduction has previously been described. The Λ^o sample is estimated to be at least 90% pure. The P_T^- distribution for all Λ^o's is shown in Figure 3b. The curve in Figure 3b is what is expected

from phase space normalized to all events.

A neutral was considered to be a $\bar{\Lambda}^o$ candidate if it was assigned a $\bar{\Lambda}^o$ identity using the procedure that was outlined for the Λ^o's and was backward in the center of mass. All $\bar{\Lambda}^o$ candidates were examined at the scan table. Using the scan information $\bar{\Lambda}^o$-γ ambiguities were resolved in favor of the $\bar{\Lambda}^o$ if there was evidence of any of the following:

1) a non-zero opening angle
2) decay of out-going track
3) out-going track interacts.

The $\bar{\Lambda}^o$-K^o ambiguities were resolved in favor of the 3c fit with the highest confidence level as calculated by SQUAW. The contamination of the $\bar{\Lambda}^o$'s is due solely to the K^o's and is estimated to be $\leq$ 20%.

The results of this section are summarized in Table 2.

V Attenuation Weights

In order to correct for the loss of γ's or V^o's which did not convert or decay in the chamber, we assign to each observed event a weight that is inversely proportional to the probability that the detected particle should be observed in a chosen fiducial volume. The probability for conversion or decay in a given path length (L_p) is:

$$1) \qquad P_{(L_p)} = e^{-L_m/L_o} - e^{-L_p/L_o} .$$

Here, L_o is the mean conversion or decay length and L_m is the minimum length allowed between the primary and secondary vertex. The values of

FERMILAB-CONF-78-123-E

of L_o for γ's were taken from References 6 and 7. The values of L_o for the V^o's are easily calculated from the mean lifetime.[8] The average weights for K_s^o's, Λ^o's, and $\bar{\Lambda}^o$'s backward in the center of mass are 1.38, 1.32 and 1.19 respectively. The average weight for the γ's (both center of mass hemispheres) is 9.14.

VI Symmetry Correction for γ

The fact that the pair production cross section is essentially constant above a few GeV means the detection efficiency of γ's should be approximately equal for the two hemispheres in the center of mass. This is in sharp contrast to the strange particles, for which the detection efficiency in the forward center of mass hemisphere is quite poor due to time dilation. Experimentally we find that there is a loss of γ's with both very low and very high laboratory momenta. In order to study these losses and correct for them, we exploit the forward-backward symmetry of pp collisions in the center-of-mass frame.

The losses at low momentum are due to γ's which are: a) hard to find on scan table since the electron and positron spirals are small; b) susceptible to reconstruction losses in TVGP since the spirals are tight, and not many points can be measured on the track; and c) more likely to undergo compton scattering than pair production.

Figure 4 is a scatter plot of the longitudinal momentum in the center of mass (P_L^{cm}) vs. the transverse momentum (P_T) for γ's (Peryou plot). The curve on the left hand side corresponds to boundary of the phase space that would be populated by γ's with $E_{lab} \leq 60$ MeV. The curve on

the right is the reflection of this boundary. We see that the distribution at small P_T is not symmetric due to the low-momentum losses.

To further investigate these losses, we examined the weighted (attenuation weight) laboratory energy distribution of γ's (Figure 5). In order to estimate the original shape of this distribution, "fake" γ's were produced by approximating the π^o momentum distribution with the measured π^- distribution. The π^o was then assumed to decay isotropically in its own rest frame into two γ's, and the γ's four-momenta were transformed back to the laboratory frame. The resulting energy distribution is shown in Figure 6. A comparison with Figure 5 shows that there are severe losses for $E_\gamma \leq 60$ MeV.

In order to correct for the low-momentum losses when calculating cross sections, events with $E_{lab} \leq 60$ MeV were assigned a weight of zero, while events lying in the reflected region of the Peyrou plot had their weights doubled.

High momentum γ's may be lost in scanning and measuring since the conversion space point may be obscured by the hadron jet and the e^+ and e^- tracks may be indistinguishable from the hadron tracks.

The losses in the forward center of mass hemisphere were studied by making use of the forward-backward symmetry of the γ center of mass rapidity (y^*) distribution. Assuming that the efficiency for processing a γ in the backward hemisphere is $\approx$ 100% (neglecting γ's with $E \leq 60$ MeV) we can obtain the corrections needed for the forward hemisphere.

After first deleting the events under the curves of Figure 4, we construct the ratio, $R(|y^*|) = F/B$, where F is the weighted number of γ's within an interval Δy with $y^* > 0$ and B is the number on the corresponding

interval with $y^* = -|y^*|$. Since the losses in the jet may be multiplicity dependent, this ratio was plotted for four different groups: a) 2, 4, 6 prongs, b) 8, 10 prongs, c) 12, 14 prongs, and d) > 14 prongs, with each group divided into 4 or 5 rapidity intervals. Within statistics, all distributions were consistent with the same linear decrease in R. The result of a least squares fit to the combined data (Figure 7a) is:

$$R = 1 + A|y^*| \qquad A = -.142 \pm .0237$$

$$\frac{\chi^2}{D.O.F.} = 1.17$$

Figure 7b shows the R distribution that results from applying this linear correction.

VII Charged Particle Cross Sections

The charged particle cross sections were obtained by scanning the film and recording the number of charged prongs (multiplicity) for each event. The number of events with three or more prongs is listed in Table 3. Two-prong events are not considered here since the scanning efficiency for them is low (∿ 90%) due to the loss of short proton tracks caused by the large chamber-to-film demagnification. Events with an odd number of prongs were classified as even prongs according to the following scheme:

1) add one to the multiplicity if the prong number was ≤ 7.
2) subtrack three[9] from the multiplicity if the prong number was ≥ 9.

The number of events after making this correction is listed in the third column of Table 3. The topological cross sections, σ_n, were calculated using

2) $$\sigma_N = N \cdot \frac{\sigma_{>4}}{N_T} .$$

Here, N_T is the total number of events (5105), $\sigma_{>4}$ is the cross section to produce $\geq$ 4 charged prongs (30.1 $\pm$ 1 mb from Reference 10), and N is the number of events of a given multiplicity. The cross sections are listed in Table 3.

The topological cross sections are in agreement with those of Ref. 10. Some low order moments of the multiplicity distribution are presented in Table 4. These quantities are calculated in terms of N_-, the number of negative tracks in an event.

The average number of negative particles per inelastic collision ($\langle N_- \rangle$) increases by approximately 40% when the laboratory momentum changes from 100 GeV/c to 400 GeV/c. The correlation parameter, f_2^{--} ($\equiv \langle N_-(N_--1)\rangle - \langle N_-\rangle)^2$, increases rapidly in this momentum range, growing from a value of 0.28 at 102 GeV/c to 2.14 at 400 GeV/c.

VIII Cross Sections for π^o, K^o, Λ^o, $\bar{\Lambda}^o$.

In this section we consider the following reactions:

FERMILAB-CONF-78-123-E

a) $pp \rightarrow \pi^o X$

b) $pp \rightarrow K^o X$

c) $pp \rightarrow \Lambda^o X$

d) $pp \rightarrow \bar{\Lambda}^o X$.

Cross sections were calculated as follows:

$$\sigma_i = \frac{\sigma_{IN} \cdot N_i}{N_T} ,$$

where σ_{IN} is the inelastic cross section from Ref. 10, N_T is the total number of events in the sample, and N_i is the weighted number of particles of type i ($i = \pi^o, K^o, \Lambda^o, \bar{\Lambda}^o$). Only particles backward in the center of mass were used in obtaining cross sections for neutral strange particle production. Corrections were made for unseen decay modes. The π^o cross section was obtained from the γ cross section through

$$\sigma_{\pi^o} = \sigma_\gamma/2.$$

The inclusive and semi-inclusive cross sections for these reactions are listed in Table 5. Figs. 8-11 show these cross sections as a function of incident proton laboratory momentum.[11-20]

The π^o cross section is rising as a function of incident momentum, as predicted by most multiperipheral models (Fig. 8). At the highest energies, however, the cross section appears to deviate from the expected $\ell n s$ behavior.

The neutral pion cross section can be compared (curves in Fig. 8) with the charged pion cross section (σ_{π^+}, σ_{π^-}) using the data of Ref. 21. We find

$$\sigma_{\pi^o}(142.3 \pm 6.2 \text{ mb}) > \sigma_{\pi^+}(128 \text{ mb}) > \sigma_{\pi^-}(107 \text{ mb}).$$

Since the parameterizations for σ_{π^+} and σ_{π^-} are expected to be accurate only to $\sim$ 10%, one could argue that σ_{π^o} is consistent with σ_{π^+}. It is definitely inconsistent with σ_{π^-}, however.

In the hundred GeV range we see that σ_{K^o} is only slightly energy dependent, in marked contrast to its behavior at lower energies (Fig. 9). The behavior of σ_{Λ^o} [22] (Fig. 10) is similar to that of σ_{K^o} over most of the momentum range under consideration. However, σ_{K^o} and σ_{Λ^o} are not related by a simple change of scale since σ_{K^o} rises faster than σ_{Λ^o}. In addition, σ_{Λ^o} does not show any energy dependence in the hundred GeV range.

There are 4 events of the type

$$pp \rightarrow K_s^o K_s^o X$$

with both K_s^o's backward in the center of mass. These 4 events correspond to a cross section of $.16 \pm .09$ mb. Two of these events have $m_{K^oK^o} <$ 1.1 GeV/c^2 suggesting that a substantial fraction of the K_s^o pairs are produced near threshold.

The dependence of $\sigma_{\bar{\Lambda}^o}$ (Fig. 11) on incident momentum is uncertain since most bubble chamber experiments with $P_{lab} > 50$ GeV/c detect fewer than 20 $\bar{\Lambda}^o$'s. What is clear is that $\sigma_{\bar{\Lambda}^o}$ is only a fraction ($\simeq$ 10% for

FERMILAB-CONF-78-123-E

this experiment) of σ_{Λ^o}. Presumably, this difference is due to proton fragmentation ($p \rightarrow K^+\Lambda^o$) which can produce Λ^o's but not $\bar{\Lambda}^o$'s.

A question of interest is how much of the $\bar{\Lambda}^o$'s are the result of $\Lambda^o\bar{\Lambda}^o$ production. In this experiment there are three events with a $\Lambda^o\bar{\Lambda}^o$ pair, both particles being backward in the center of mass. These three events correspond to a cross section of $\sigma_{\Lambda^o\bar{\Lambda}^o} = .12 \pm .07$ mb. A sizeable fraction of the $\bar{\Lambda}^o$'s are thus produced in association with a Λ^o. All three pairs are produced in the central region of rapidity and in all cases

$$|Y_{\Lambda^o} - Y_{\bar{\Lambda}^o}| < 1 .$$

In summary, we have seen that the neutral strange particle cross sections are at most only slightly energy dependent in the hundred GeV range, while the π^o cross section is rising at least as fast as $\ell n s$.

IX Average Number of Particles per Inelastic Collision

The average number of particles per inelastic collision for reactions a-c, $\langle\pi^o\rangle$, $\langle K^o\rangle$, and $\langle\Lambda^o\rangle$, are listed in Table 6. Figs. 12-14 show the dependence of these quantities on incident momentum.

The curve[23] in Figure 12 represents a fit of the form:

$$\langle\pi^o\rangle = a + b \log(P_{lab}) \qquad a = -.82 \pm .16$$
$$b = .79 \pm .05$$

to previously existing data. The value for $\langle\pi^o\rangle$ obtained by this experiment is somewhat higher than what is expected from this equation.

Next we turn our attention to the average number of particles for fixe N_- ($\langle A\rangle_-$). By N_-, we mean the number of negative particles in the event. In Figs. 15-17 we plot $\langle\pi^o\rangle_-$, $\langle K^o_s\rangle_-$ and $\langle\Lambda^o\rangle_-$. The behavior of $\langle A\rangle_-$ is different for mesons and baryons.

For the π^o's and K^o_s's $\langle A\rangle_-$ increases with increasing N_-. Both $\langle\pi^o\rangle_-$ and $\langle K^o\rangle_-$ can be represented by a fit of the form:

$$\langle A\rangle_- = a + bN_- \quad .$$

The results of the fits are given in table 7. In contrast to the mesons, $\langle\Lambda^o\rangle_-$ is rather flat for $N_- \geq 3$.

The strong dependence of $\langle\pi^o\rangle_-$ on N_- suggests that for some large fraction of the time, the observed π^o's and π^-'s are the products of the decay of some higher mass object. This object might be a vector meson or a "blob" of indefinite mass but fixed isospin. The concept of the massive "blob" is similar to that of proton diffraction (e.g. $p \rightarrow N\pi^+$) where the quantum numbers of the $N\pi^+$ system are fixed byt the mass of the system is not. It is also possible that the observed correlation between the π^o's and π^-'s might be accounted for by some statistical process.

In Fig. 18 the predictions for the $\langle\pi^o\rangle_-$ vs N_- for five models[24-29] of pion production are compared with the experimental data. The models considered are:

1) "π" model - single pion production
2) "ε" model - production of $\pi^+\pi^-$, $\pi^o\pi^o$ I = 0 pairs
3) "ρ" model - production of $\pi^+\pi^-$, $\pi^+\pi^o$, $\pi^-\pi^o$ I = 1 pairs
4) "ω" model - production of $\pi^+\pi^-\pi^o$ I = 0 triplets
5) "critical fluid" model - a thermodynamic model.

FERMILAB-CONF-78-123-E

All of the models considered predict a rise in the $\langle\pi^o\rangle_-$ as a function of N_-. Only the critical fluid model is in good agreement with the data, however. The ε model provides a fair description of the data if the errors associated with the predicted points are taken into consideration. The remaining three models (π, ρ, ω) are inconsistent with the data. A more detailed discussion of these models is given in section XI.

X Production of π^o, $\eta(548)$, $\omega(783)$, Σ^o, $\bar{\Sigma}^o$.

In Fig. 19a, the invariant mass distribution for γ pairs is displayed. A strong π^o signal is present. In order to enhance the π^o signal and cut out some of the low mass backgrounds ($M_{\gamma\gamma} \lesssim 120$ MeV), a minimum $\gamma\gamma$ opening angle cut was made.[30] In addition, only events that have their primary vertex in the first half of the chamber were used. This fiducial cut was made to minimize the large fluctuations in the weights of the γ pairs. In Fig. 19b, the weighted mass distribution is shown. In Figs. 19c and 19d, the unweighted and weighted mass distribution for γ pairs fitting (using SQUAW) the hypothesis

$$\pi^o \rightarrow \gamma\gamma$$

are presented. Using the events in Figs. 19c and 19d with $125 \leq M_{\gamma\gamma} < 145$ for the π^o signal, we calculate a cross section, σ_{π^o}, of 138 ± 15 mb. This is consistent with the value of 142 ± 6 mb which was obtained assuming $\sigma_{\pi^o} = \frac{1}{2}\sigma_\gamma$.

In Figs. 19a and 19b, there is no evidence for $\eta(548)$ production. An upper limit (at the 90% confidence level) for the ration $\eta(548)/\pi^o$

FERMILAB-CONF-78-123-E

can be found using the fitted π^o events (Figs. 19c and 19d). We obtain:

$$\eta(548)/\pi^o < 5\%$$

and

$$\sigma_{\eta(548)} < 7 \text{ mb}$$

90% confidence level

all decay modes included

The search for $\omega(783)$ production was made only in events with ≤ 10 prongs. All tracks were assumed to be pions unless they were identified otherwise. In order to insure that the $\pi^+\pi^-\pi^o$ combination was well measured, we use only events (unless otherwise mentioned) which satisfy:

$$\frac{\delta M_{\pi^+\pi^-\pi^o}}{M_{\pi^+\pi^-\pi^o}} < 2\%$$

δM = error in mass calculated by SQUAW

M = mass

In Figs. 20a and 20b, the unweighted and weighted mass distribution of all (the above mentioned cut is not imposed) γ pairs in events with ≤ 10 prongs is displayed. The events that fit the reaction $\pi^o \to \gamma\gamma$ (using SQUAW) and meet the above mentioned error cut are shown in Figs. 20c (unweighted) and 20d (weighted).

The invariant mass distribution for $\pi^+\pi^-\pi^o$ triplets is shown in Fig. 21. There is no obvious $\omega(783)$ signal present. In order to search further for this signal, we have also used the variable[31] $\lambda \equiv (Q/Q_{max})^2$ where Q is the matrix element of the $\omega(783)$. For a 1^- particle, $Q^2 = |\bar{K}_1 \times \bar{K}_2|^2$, where $\bar{K}$ is the momentum of a decay product in the rest frame of the $\omega(783)$ and Q_{max} is the largest value of Q. Specifying a value for λ is equivalent to specifying a region in a Dalitz plot. In a sample of pure $\omega(783)$'s, $\sim 75\%$ should have $\lambda \geq .5$. The area of the Dalitz plot

specified by $\lambda \geq .5$ is only $\sim$ 50% of the total, however, so if our events are not governed by the 1^- matrix element (i.e., are not $\omega(783)$'s), we would expect $\sim$ 50% of them to lie in the region with $\lambda \geq .5$. A histogram of λ for events with $735 \leq M_{\pi^+\pi^-\pi^0} \leq 835$ Mev is shown in Fig. 22. There is no excess of events with $\lambda \geq .5$ and we conclude that there is little if any $\omega(783)$ present. The upper limit (90% confidence level) for $\omega(783)$ production is $\frac{\omega(783)}{\pi^0} < 4.8\%$ or $\sigma_{\omega(783)} < 3$ mb. We remind the reader that these are based on events with fewer than 11 prongs. All decay modes were included and corrections were made for events with $\delta M/M > 2\%$.

The cross sections for Σ^0 and $\bar{\Sigma}^0$ production are obtained using events that fit (using SQUAW) the following reactions:

a) $\Sigma^0 \longrightarrow \Lambda^0 \gamma$, $\gamma \to e^+e^-$, $\Lambda^0 \to p\,\pi^-$

b) $\bar{\Sigma}^0 \longrightarrow \bar{\Lambda}^0 \gamma$, $\gamma \to e^+e^-$, $\bar{\Lambda}^0 \to \bar{p}\,\pi^+$

There is one event above background for each of these reactions, giving:

$$\sigma_{\Sigma^0} = .26 \text{ mb}$$

$$\sigma_{\bar{\Sigma}^0} = .22 \text{ mb} .$$

The above cross sections are for both center of mass hemispheres, and include the branching ratio of unseen decay modes.

FERMILAB-CONF-78-123-E

In Ref. 19, a cross section of 1.14 mb for charged $Y^*(1385)$ ($\rightarrow \Lambda^o\pi$ only) production was obtained. This fact, coupled with the estimate obtained for σ_{Σ^o}, suggests that $\geq \frac{1}{4}$ of the detected Λ^o's are decay products of a higher mass state.

XI Inclusive Two-Body Correlations

In this section, correlations between neutral and charged pions will be studied and compared to the predictions of the five previously mentioned models. In particular, we examine the behavior of the Mueller correlation parameters:

$$f_2^{--} = \langle N_-(N_- - 1)\rangle - \langle N_-\rangle^2$$

$$f_2^{o} = \langle N_o N_-\rangle - \langle N_o\rangle\langle N_-\rangle$$

$$f_2^{oo} = \langle N_o(N_o - 1)\rangle - \langle N_o\rangle^2 \quad .$$

When calculating f_2^{o-} and f_2^{oo}, we assume that

$$N_o = N_\gamma/2 \ .$$

We can now rewrite f_2^{oo} as

$$f_2^{oo} = \frac{1}{4}\,[\langle N_\gamma(N_\gamma - 1)\rangle - \langle N_\gamma\rangle^2] - \frac{\langle N_\gamma\rangle}{4} = \frac{1}{4}\,f_2^{\gamma\gamma} - \frac{1}{4}\,\langle N_\gamma\rangle \ .$$

Table 8 lists the values of f_2^-, f_2^{o-} and f_2^{oo}. The ordering of the parameters $f_2^{--} < f_2^{o-} < f_2^{oo}$ implies that π^o's are more correlated than π^-'s. The semi-inclusive scaling law of Ref. 32 leads to the prediction that at high energyies, $f_2^{--} > f_2^{o-}$. The data do not support this prediction.

The incident momentum dependence[10-19,33-36] of the three correlation parameters is displayed in Figs. 23a-c. All parameters are increasing with increasing incident momentum.

In order to explain the observed correlations at 400 GeV/c, we now consider the five models of pion production. These models allow one to calculate f_2^{o-} and f_2^{oo} in terms of the well-measured quantities, f_2^{--} and $\langle N_- \rangle$. The results are displayed in Figs. 25a and 24b. Of the models considered, the critical fluid model shows the best agreement with the data. No model having only one type of cluster with definite isospin fits all data. It would be possible, however, to fit the data with a model incorporating two or more clusters of definite isospin (e.g., a "$\rho + \varepsilon$" model).

XII Conclusion

We have presented results on charged and neutral particle production from pp collisions at 400 GeV/c. The main results are the following:

a) Inclusive and semi-inclusive measurements of π^o, K_s^o, Λ^o, $\bar{\Lambda}^o$, Σ^o and $\bar{\Sigma}^o$ have been made. The π^o cross section is rising at least as fast as ℓns. The K^o cross section also appears to increase at Fermilab energies. In contrast, the Λ^o cross section is constant at Fermilab energies. The average number of π^o's and K^o's increases as a function of the number of negative particles in an event. No such dependence is found for the Λ^o's.

b) From the events with two or more converted γ's, upper limits are calculated for inclusive $\eta^o(548)$ production and, for events with fewer than 11 prongs, $\omega^o(783)$ production.

FERMILAB-CONF-78-123-E

c) Neutral and charged pion correlations were studied in terms of $\langle\pi^o\rangle_-$ and the Mueller moments, f_2^{--}, f_2^{o-}, and f_2^{oo}. Predictions from five models of pion production were compared with the data. Of these, only the Critical Fluid model is in good agreement with the data.

XIII Acknowledgements

We thank the Fermilab 15 foot bubble chamber personnel for their help in obtaining the pictures. The careful work by the scanning and measuring personnel at U.C. Davis and LBL is greatly appreciated.

Table 1

P_T^- (MeV/c)	γK^o	$\gamma \Lambda^o$	$\gamma \bar{\Lambda}^o$	$K^o \Lambda^o$	$K^o \bar{\Lambda}^o$	$\Lambda^o \bar{\Lambda}^o$	$\gamma K^o \Lambda^o$	$\gamma K^o \bar{\Lambda}^o$	$\gamma \Lambda \Lambda^o$	$K^o \Lambda^o \bar{\Lambda}^o$	$\gamma K^o \Lambda^o \bar{\Lambda}^o$
0 → 20	51	57	85	0	0	0	4	3	0	0	1
20 → 40	5	16	8	0	0	0	2	1	0	0	0
40 → 102	8	52	10	10	5	0	13	8	0	0	0
102 → 206	57	0	0	3	0	0	12	6	0	0	0
Overlap	0	8	11	0	0	0	2	0	0	0	0
Totals	121	133	114	13	5	0	33	18	0	0	1

Listing of 3c fit ambiguities. The P_T^- refers to the transverse momentum of the π^- when a K^o is involved, π^- of Λ^o for $\gamma\Lambda^o$ ambiguities, and $\bar{p}$ for $\gamma\bar{\Lambda}^o$ ambiguities. The overlap events are those events which have P_T^- of the V^o > 20 MeV/c and P_T^- of the γ < 20 MeV/c.

Table 2

	γ	K^o	Λ^o
Unique	2468	180	44
Resolved	222	91	93
Totals	2690	271	137

Summary of 3c fits for γ, K^o and Λ^o.
The $\bar{\Lambda}^o$ were treated separately.

TABLE 3

Topological Cross Sections at 400 GeV/c

Prong Number	Number Observed	Corrected Number	Cross Section (mb)
3	16		
4	727	743	4.38 ± .20
5	13		
6	866	888	5.24 ± .23
7	11		
8	831	854	5.04 ± .22
9	9		
10	798	802	4.73 ± .21
11	12		
12	651	666	3.93 ± .19
13	4		
14	473	477	2.81 ± .15
15	5		
16	341	342	2.02 ± .12
17	4		
18	163	165	.97 ± .08
19	1		
20	87	87	.51 ± .057
21	2		
22	39	41	.24 ± .038
23	0		
24	23	23	.14 ± .029
25	2		
26	6	6	.035 ± .015
27	0		
28	7	8	.047 ± .017
29	0		
30	3	3	.018 ± .010
31	1		

TABLE 4

Low Order Moments of Multiplicity Distribution

	All* Prongs	≥4 Prongs
$\langle N_- \rangle$	3.57 ± .03	3.89 ± .03
$\langle N_-^2 \rangle$	18.44 ± .30	20.10 ± .31
f_2^{--}	2.14 ± .11	1.09 ± .10

*The number of inelastic two prongs was calculated using the inelastic two prong cross section 2.7 ± .1 mb from Reference 2.

Table 5

Prongs	π^o Events	σ_{π^o}	K^o_s Events	$\sigma_{K^o_s}$	Λ^o Events	σ_{Λ^o}	$\bar{\Lambda}^o$ Events	$\sigma_{\bar{\Lambda}^o}$
2	103	5.07 ± .93	5	.17 ± .12	3	.10 ± .08	0	-
4	225	11.49 ± 1.52	15	.55 ± .22	11	.35 ± .15	0	-
6	402	18.62 ± 1.89	30	.98 ± .27	20	.71 ± .24	3	.09 ± .07
8	490	21.80 ± 1.98	29	.93 ± .25	28	.94 ± .26	2	.06 ± .06
10	507	21.25 ± 1.82	33	1.00 ± .26	18	.59 ± .20	4	.12 ± .09
12	485	22.94 ± 2.13	35	1.21 ± .33	12	.37 ± .15	2	.07 ± .07
14	369	15.76 ± 1.63	22	.80 ± .27	11	.36 ± .16	1	.03 ± .03
16	276	11.67 ± 1.35	20	.63 ± .20	8	.26 ± .13	2	.06 ± .06
18	161	7.34 ± 1.17	4	.12 ± .08	4	.13 ± .09	0	-
20	78	2.76 ± .55	5	.14 ± .09	3	.10 ± .08	0	-
22	47	2.08 ± .67	3	.089 ± .073	1	.03 ± .03	0	-
24	15	.75 ± .36	0	-	1	.03 ± .03	0	-
26	9	.34 ± .22	0	-	0	-	0	-
28	8	.27 ± .17	0	-	0	-	0	-
30	2	.18 ± .18	0	-	0	-	0	-
Total	3177	142.3 ± 6.2	201	6.61 ± .73	120	3.97 ± .54	14	.42 ± .16

Inclusive Topological Cross Sections

Table 6

Prongs	π^o Events	π^o $\langle\pi^o\rangle$	K^o_s Events	K^o_s $\langle K^o_s\rangle$	Λ^o Events	Λ^o $\langle\Lambda^o\rangle$	$\bar{\Lambda}^o$ Events	$\bar{\Lambda}^o$ $\langle\bar{\Lambda}^o\rangle$
2	103	1.90 ± .24	5	.064 ± .032	3	.037 ± .022	0	-
4	225	2.53 ± .23	15	.12 ± .03	11	.076 ± .02	0	-
6	402	3.54 ± .24	30	.19 ± .04	20	.13 ± .03	3	.017 ± .010
8	490	4.32 ± .25	29	.18 ± .03	28	.19 ± .04	2	.011 ± .008
10	507	4.48 ± .24	33	.21 ± .04	18	.13 ± .03	4	.026 ± .013
12	485	5.92 ± .35	35	.31 ± .06	12	.10 ± .03	2	.017 ± .012
14	369	5.78 ± .36	22	.29 ± .07	11	.13 ± .04	1	.011 ± .011
16	276	5.96 ± .41	20	.32 ± .07	8	.13 ± .05	2	.030 ± .021
18	161	7.34 ± .72	4	.12 ± .06	4	.13 ± .06	0	-
20	78	5.34 ± .59	5	.27 ± .11	3	.20 ± .12	0	-
22	47	8.29 ± 1.78	3	.35 ± .20	1	.12 ± .12	0	-
24	15	5.68 ± 1.63	0	-	1	.22 ± .22	0	-
26	9	10.95 ± 3.16	0	-	0	-	0	-
28	8	6.01 ± 2.03	0	-	0	-	0	-
30	2	9.06 ± 4.63	0	-	0	-	0	-
Total	3177	4.34 ± .10	201	.20 ± .02	120	.12 + ± .01	14	.013 ± .003

Average Number of π^o, K^o_s, Λ^o, $\bar{\Lambda}^o$ per Inelastic Collision.

Table 7

	a	b	χ^2/D.O.F.
π^o	2.05 $\pm$ .15	.65 $\pm$ .04	1.39
K_s^o	.078 $\pm$ .022	.037 $\pm$ .007	.34

Results of the fit to $\langle A \rangle_- = a + bN_-$

Table 8

f_2^{--}	$2.14 \pm .11$
f_2^{o-}	$3.28 \pm .24$
f_2^{oo}	4.81 ± 1.38

Two-Body Correlation Moments

Footnotes and References

1) See for example, J. Whitmore, Multiparticle Production in the Fermilab Bubble Chamber, Physics Report (1976).

2) For further details of this experiment see R. Kass, Ph.D. thesis, University of California, Davis, 1978 (unpublished).

3) J. Erwin, et al., Nucl. Inst. and Meth., 148, 403 (1978).

4) W. Michael, et al., "Cicero", UCID-3880 (1977).

5) The coordinate system is such that the beam is in the positive X direction, Z is vertical and $\bar{Y} = \bar{Z} \times \bar{X}$.

6) Hubbell, NBS-29 (1969).

7) T.M. Knasel, DESY Reports Nos. 70/2 and 70/3 (1970) (unpublished).

8) Review of Particle Properties, April 1976.

9) The average multiplicity of secondaries is ~ 4.

10) C. Bromberg, et al., Phys. Rev. Lett. 31, 1563 (1973).

11) K. Jaeger, et al., Phys. Rev. D11, 1756 (1975). Data at 12.4 GeV/c.

12) H. Bøggild, et al., Nucl. Phys. B72, 221 (1974). Data at 19 GeV/c.

13) V. Blobel, et al., Nucl. Phys. B69, 454 (1972). Data at 24 GeV/c.

14) M. Boratay, et al., Nucl. Phys. B111, 529 (1976).
H. Blumenfeld, et al., Phys. Lett. 45B, 528 (1973). Data at 69 GeV/c.

15) M. Alston-Garnjost, et al., Phys. Rev. Lett. 35, 142 (1975). Data at 100 GeV/c.

16) J.W. Chopman, et al., Phys. Lett. 47B, 465 (1973). Data at 102 GeV/c.

17) K. Jaeger, et al., Phys. Rev. D11, 2405 (1975). Data at 205 GeV/c.

18) A. Sheng, et al., Phys. Rev. D11, 1733 (1975). Data at 300 GeV/c.

19) F.T. Dao, et al., Phys. Rev. Lett. 30, 1151 (1973). Data at 303 GeV/c.

20) Kichimi, et al., Phys. Lett. 72B, 411 (1978). Data at 405 GeV/c.

21) Antinucci, et al., Lettere al Nuovo Cimento, 6, 121 (1973). The authors parameterize the average number of particles per inelastic collision as a function of s. For charged pions they obtain:

$$\langle\pi^+\rangle = -1.7 \pm .3 + (.84 \pm .07)\ \ell ns + \frac{(1.0 \pm .5)}{\sqrt{s}}$$

$$\langle\pi^-\rangle = -2.6 \pm .2 + (.87 \pm .05)\ \ell ns + \frac{(2.7 \pm .4)}{\sqrt{s}} \quad .$$

This parameterization is estimated to be accurate to within 10%. The cross sections can be calculated using e.g. $\sigma_{\pi^+} = \langle\pi^+\rangle\ \sigma_{in}$ with σ_{in} taken from ref. 10. Using this prescription, we obtain:

$$\sigma_{\pi^+} = 128 \text{ mb}, \quad \sigma_{\pi^-} = 107 \text{ mb}.$$

22) Some of these $\Lambda^o(\bar{\Lambda}^o)$ may be decay products of Σ^o's ($\bar{\Sigma}^o$'s).

23) J. Whitmore, Phys. Reports 10C, 273 (1974).

24) R.C. Arnold and G. H. Thomas, Phys. Lett. 47B, 371 (1973).

25) G.H. Thomas, Phys. Rev. D8, 3042 (1973).

26) D. Drijard and S. Pokorski, Phys. Lett. 43B, 509 (1973).

27) E.L. Berger, et al., Phys. Rev. D7, 1412 (1973).

28) D. Horn and A. Schwimmer, Nucl. Phys. B52, 627 (1973).

29) P. Grassberger and H.I. Miettinen, Nucl. Phys. B82, 26 (1974).

30) For a π^o of laboratory energy E, the minimum opening angle (ϕ) between the two γ's is:

$$\cos(\phi/2) = \sqrt{1 - \left(\frac{M_{\pi^o}}{E}\right)^2} \qquad M_{\pi^o} = \text{rest mass of } \pi^o.$$

31) Trilling-Goldhaber Group, Internal Memo #62, 10/7/63.

32) F.T. Dao and J. Whitmore, Phys. Lett. B46, 252 (1973).

33) V.V. Ammosov, et al., Phys. Lett. B42, 519 (1972). Data at 50 and 69 GeV/c.

34) G. Charlton, et al., Phys. Rev. Lett. 29, 515 (1972). Data at 205 GeV/c.

35) A. Firestone, et al., Phys. Rev. D10, 2080 (1974). Data at 300 GeV/c.

36) F.T. Dao, et al., Phys. Rev. Lett. 29, 1627 (1972). Data at 303 GeV/c.

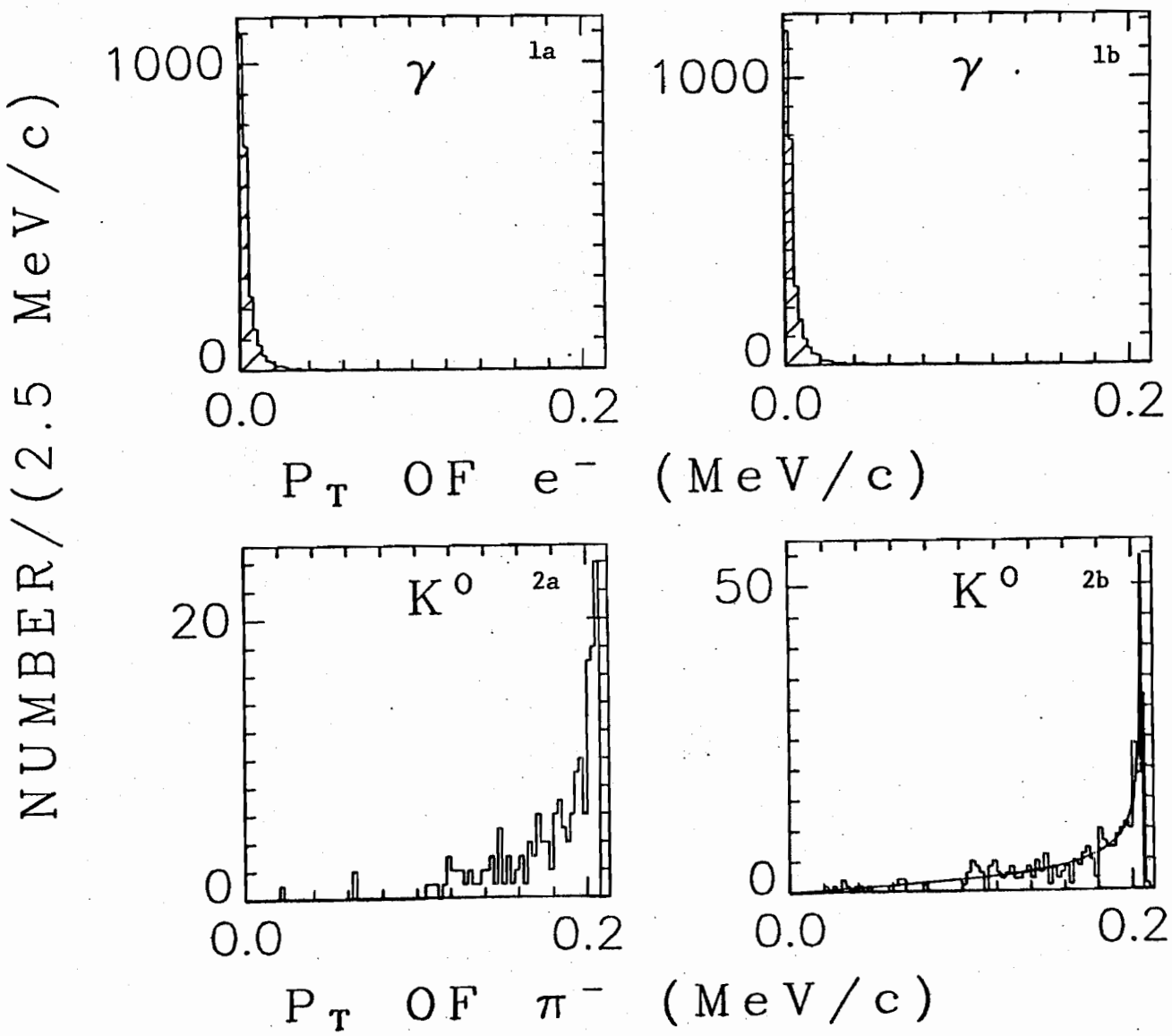

Figure 1a: Transverse momentum distribution of negative decay product relative to line of flight of its parent (P_T^-) for neutrals which fit only the γ hypothesis.

Figure 1b: P_T^- distribution for all γ's (unique and resolved).

Figure 2a: P_T^- distribution for K^o's with a unique 3c fit.

Figure 2b: P_T^- distribution for all K^o's (unique and resolved). The curve is what is expected from phase space normalized to events with $P_T^- > 102$ MeV/c.

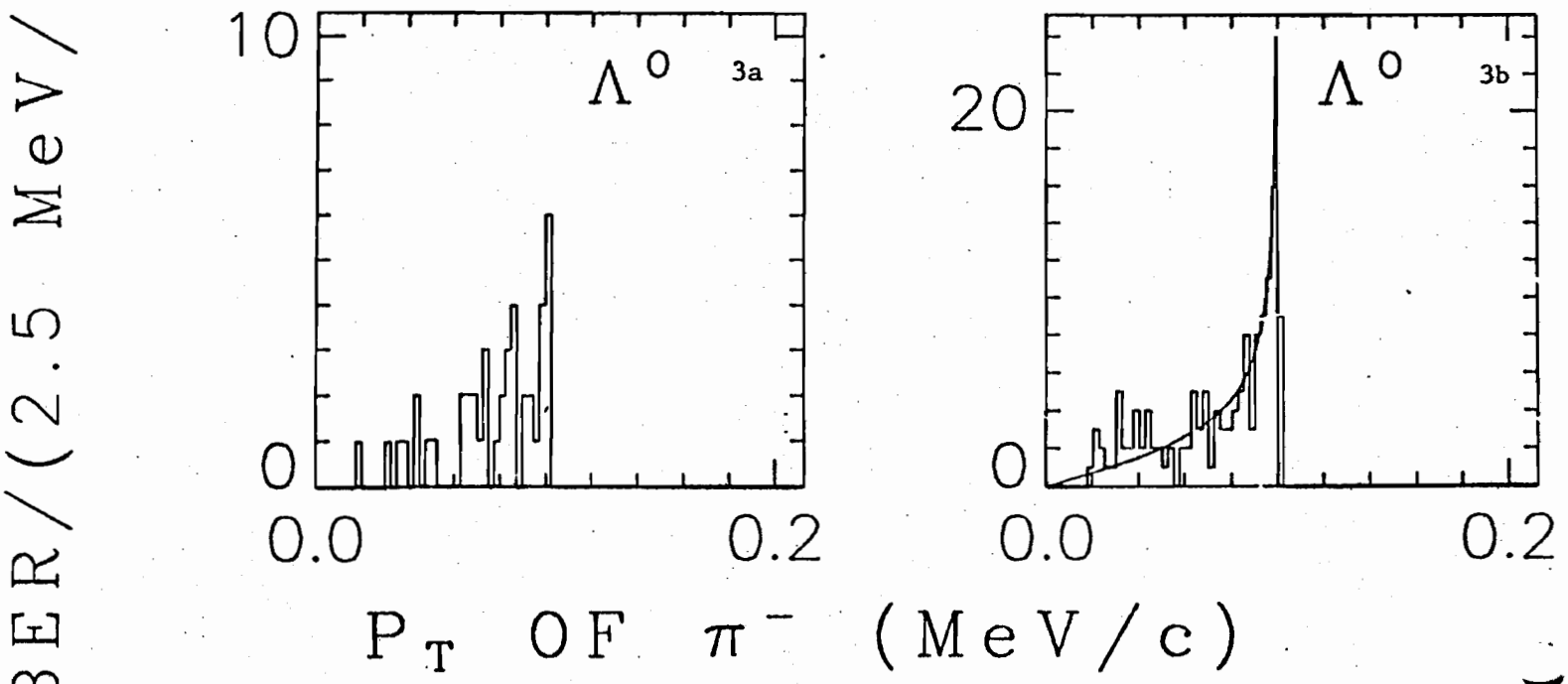

Figure 3a: P_T^- distribution for Λ^0's with a unique 3c fit.

Figure 3b: P_T^- distribution for unique and resolved Λ^0's. The curve is what is expected from phase space normalized to all events.

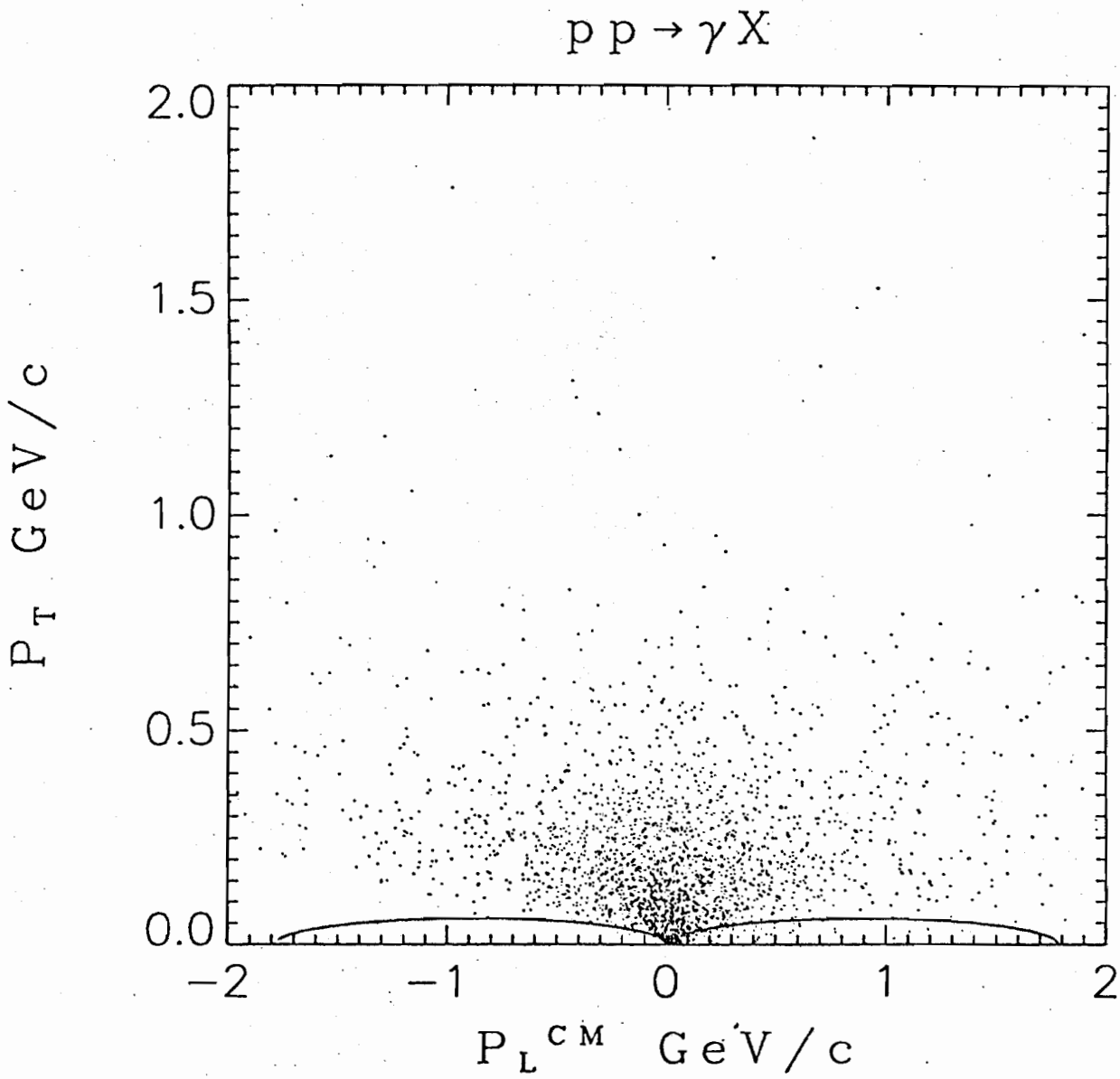

Figure 4

γ Peryou plot. The curve corresponds to

P_{LAB} = 60 MeV/c.

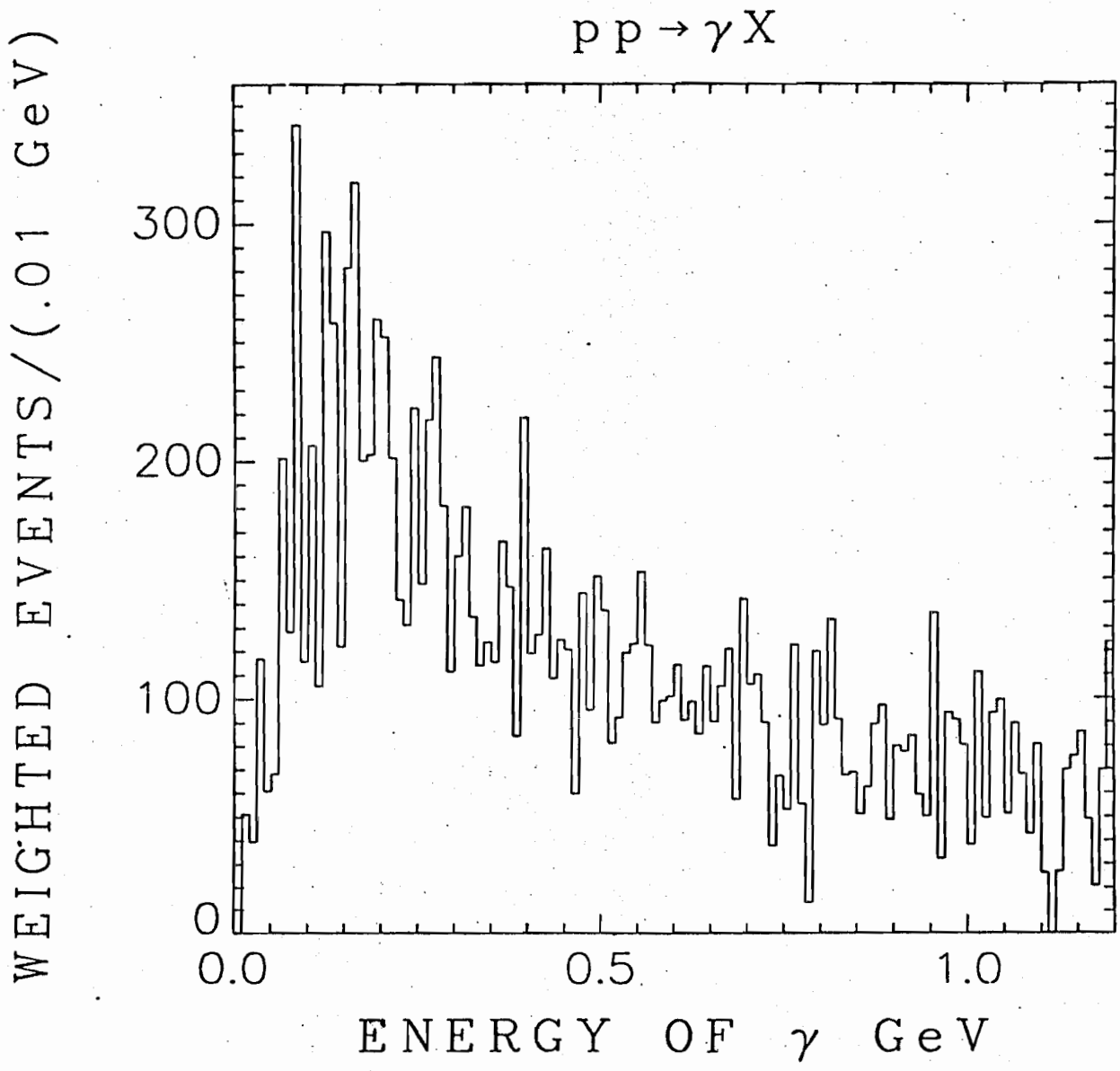

Figure 5

Laboratory energy distribution for γ's.

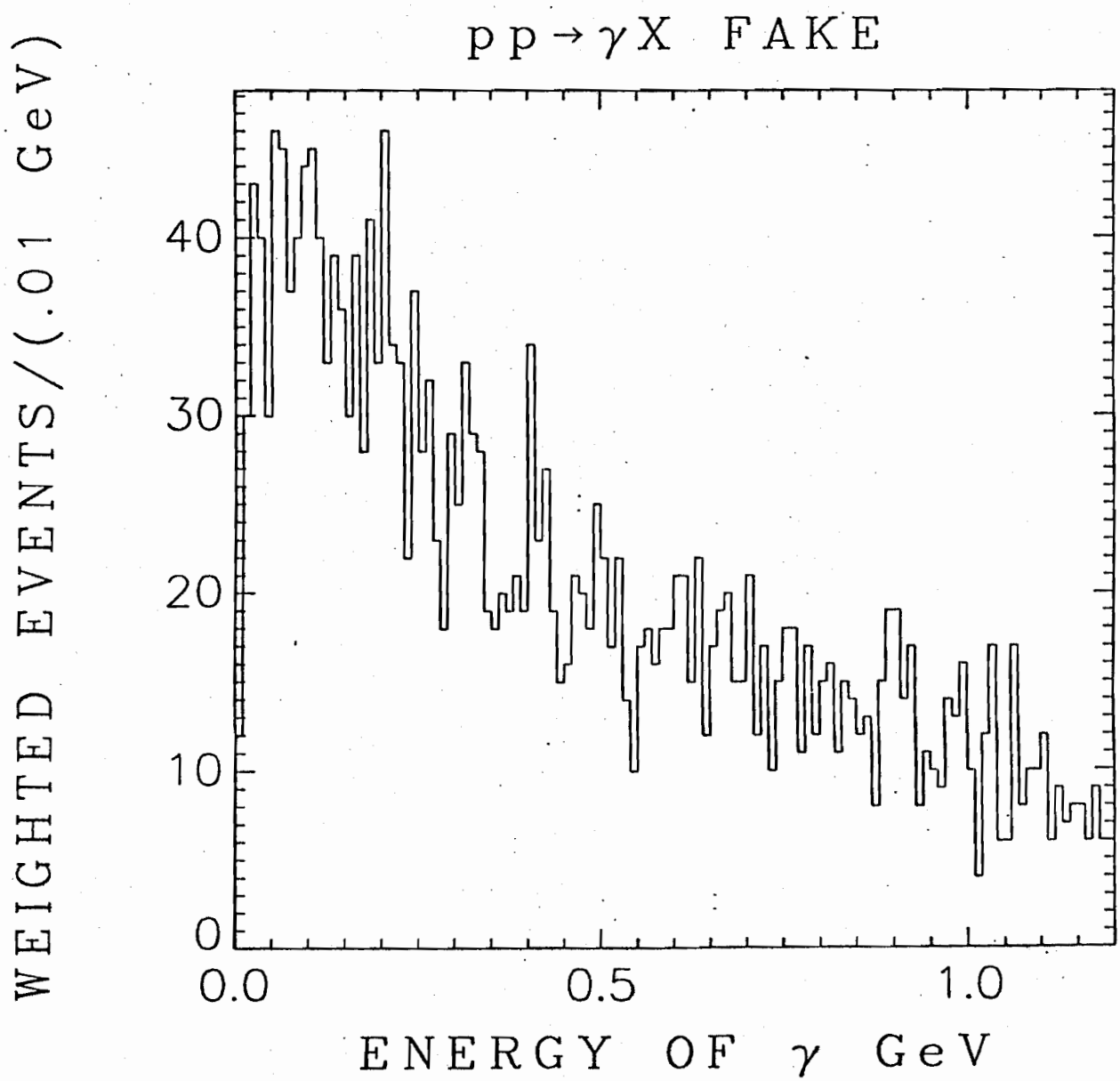

Figure 6

Laboratory energy distribution for "fake" γ's. The fake γ's were produced by assuming that the π^o momentum distribution could be approximated by the measured π^- distribution. The π^o then decayed isotropically in its own rest frame into two γ's, and the γ's four momenta were transformed back to the laboratory frame.

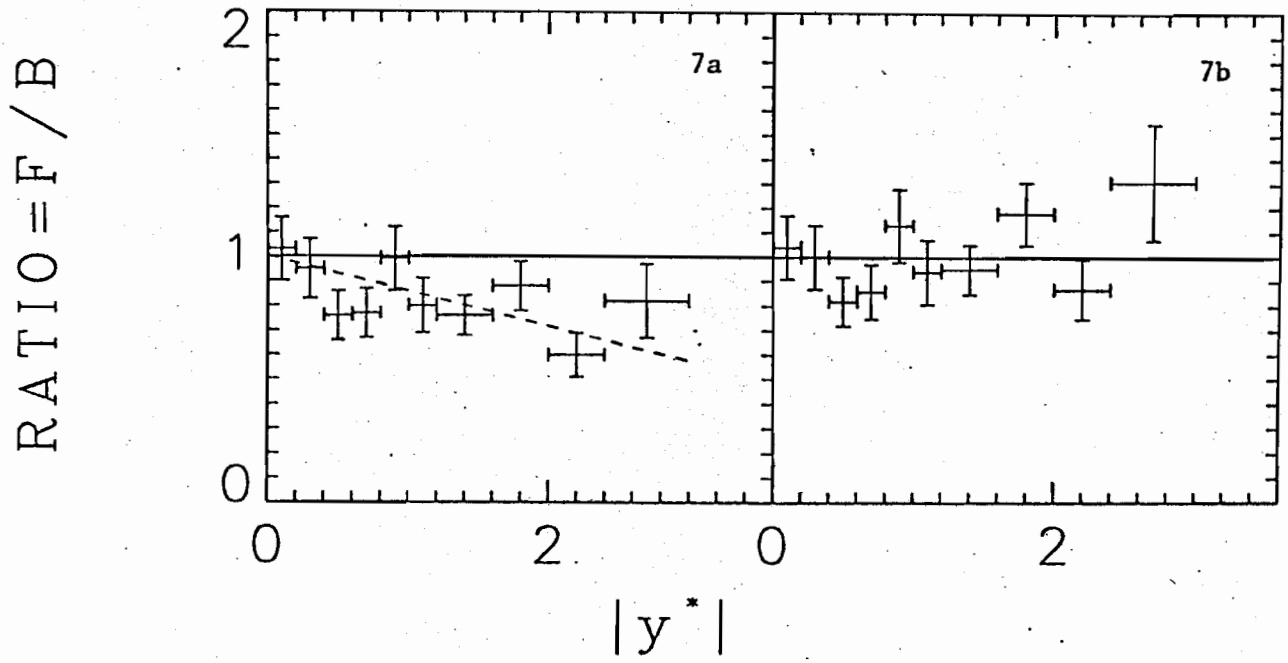

Figure 7

7a) Ratio of number of γ's in forward center of mass hemisphere to the number of γ's in the backward hemisphere. The dotted curve is a least square fit to the points.

7b) Ratio of forward to backward γ's after applying correction.

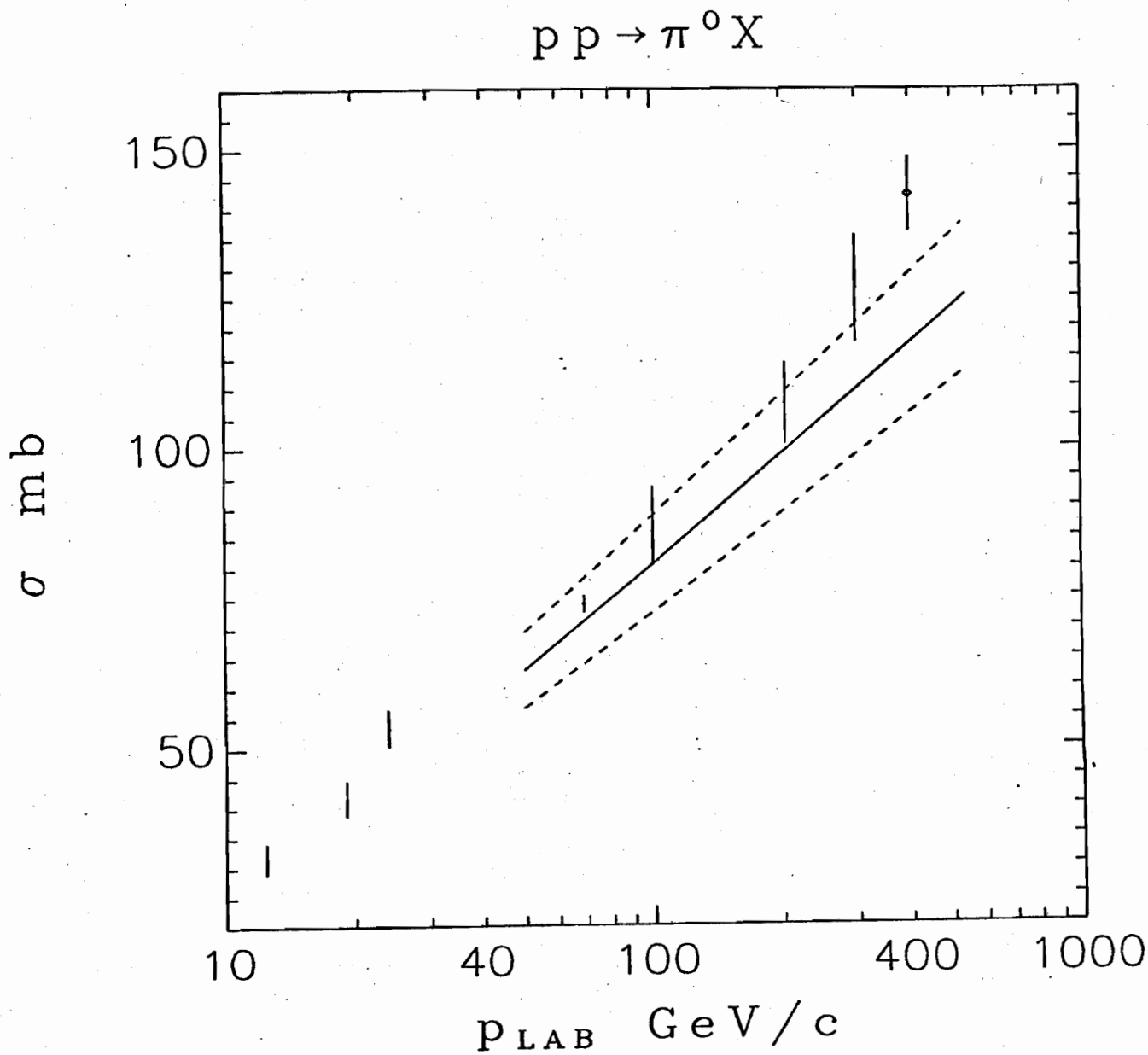

Figure 8

Inclusive cross section for π^o production as a function of incident laboratory momentum. ◇ = this experiment. The solid curve is an estimate (Ref.21) of $\frac{\sigma_{\pi^+} + \sigma_{\pi^-}}{2}$. The dashed curves are 10% upper and lower limits of the solid curve.

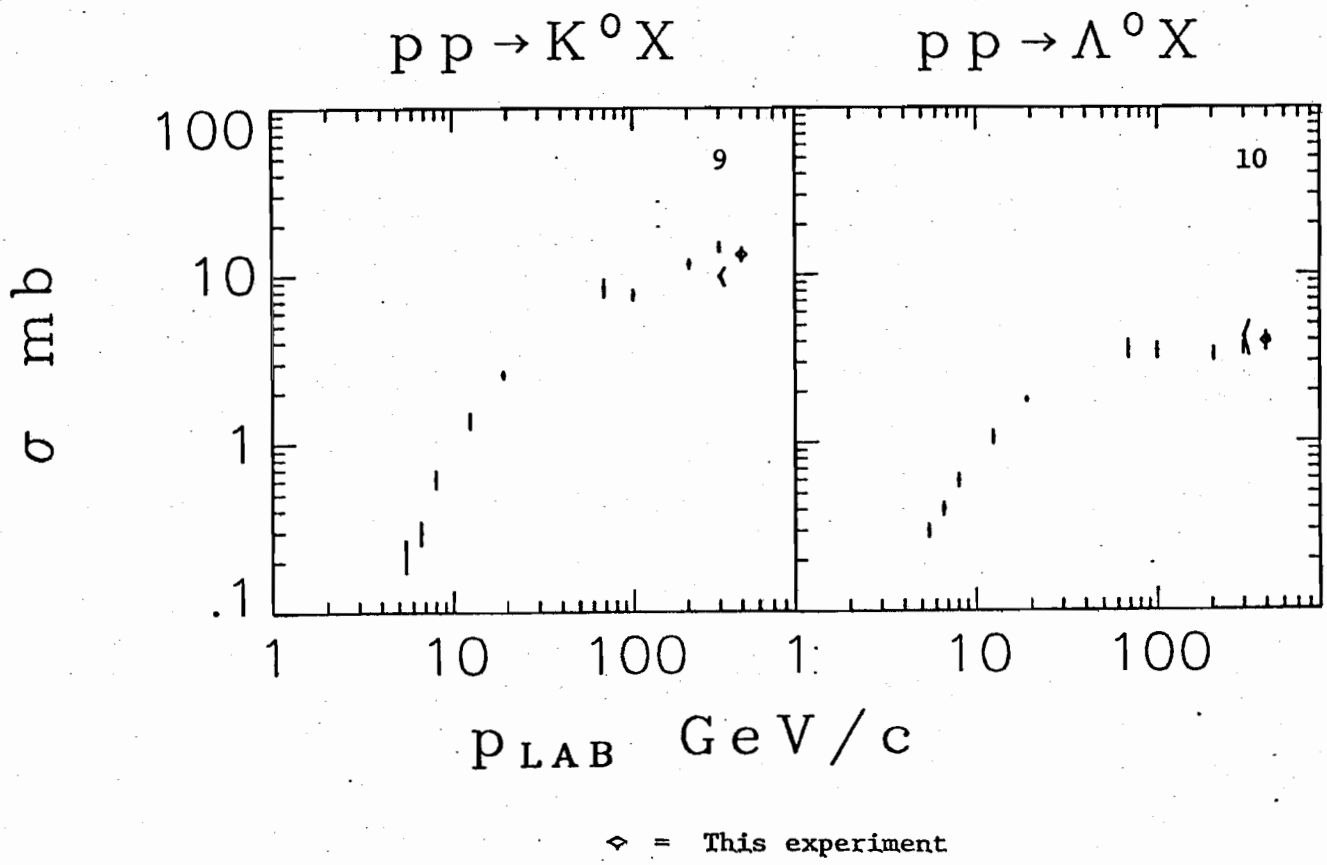

Figure 9: Inclusive K^o cross section as a function of incident laboratory momentum.

Figure 10: Inclusive Λ^o cross section as a function of incident laboratory momentum.

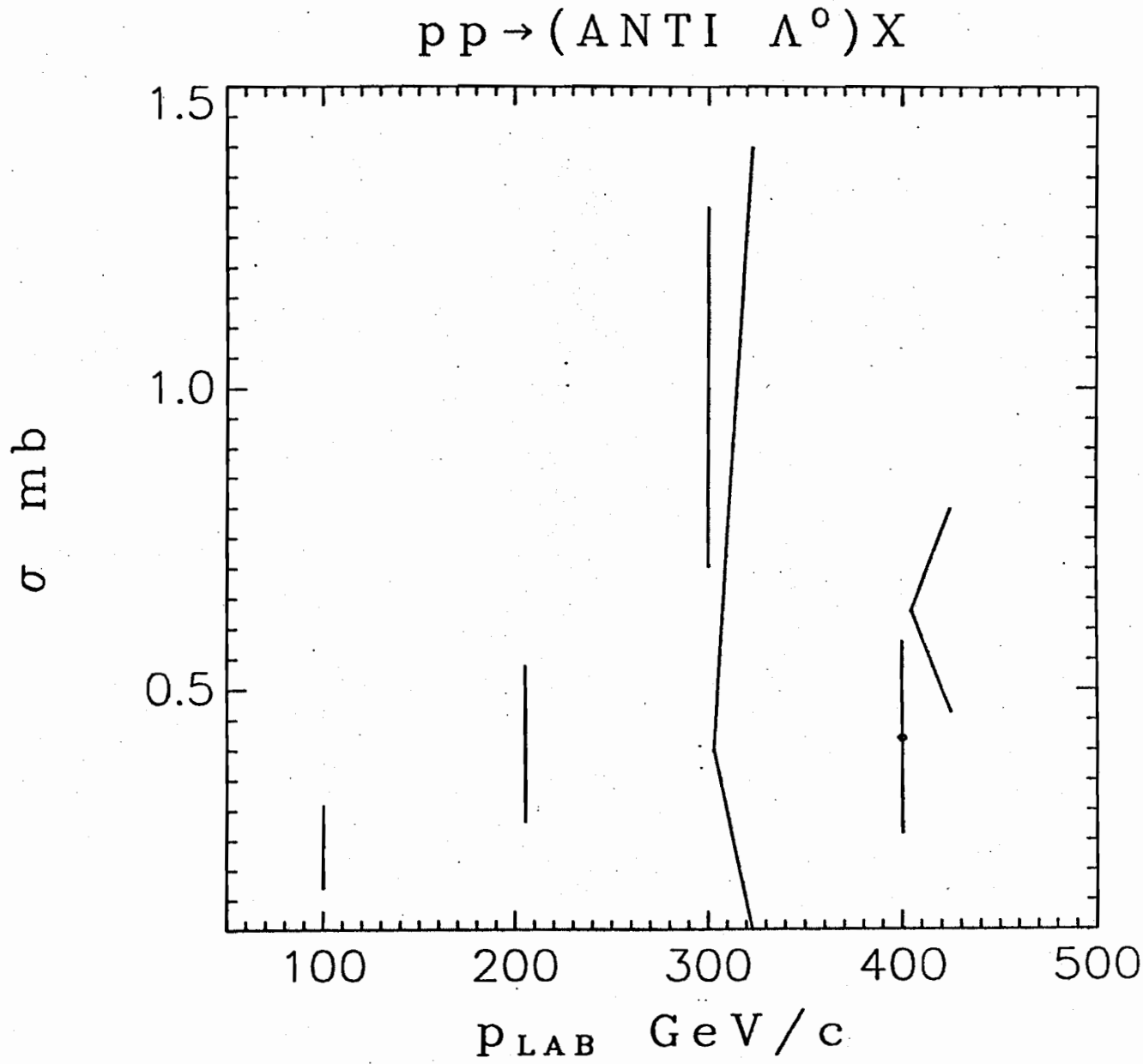

Figure 11

Inclusive $\bar{\Lambda}^{o}$ cross section as a function of incident laboratory momentum.

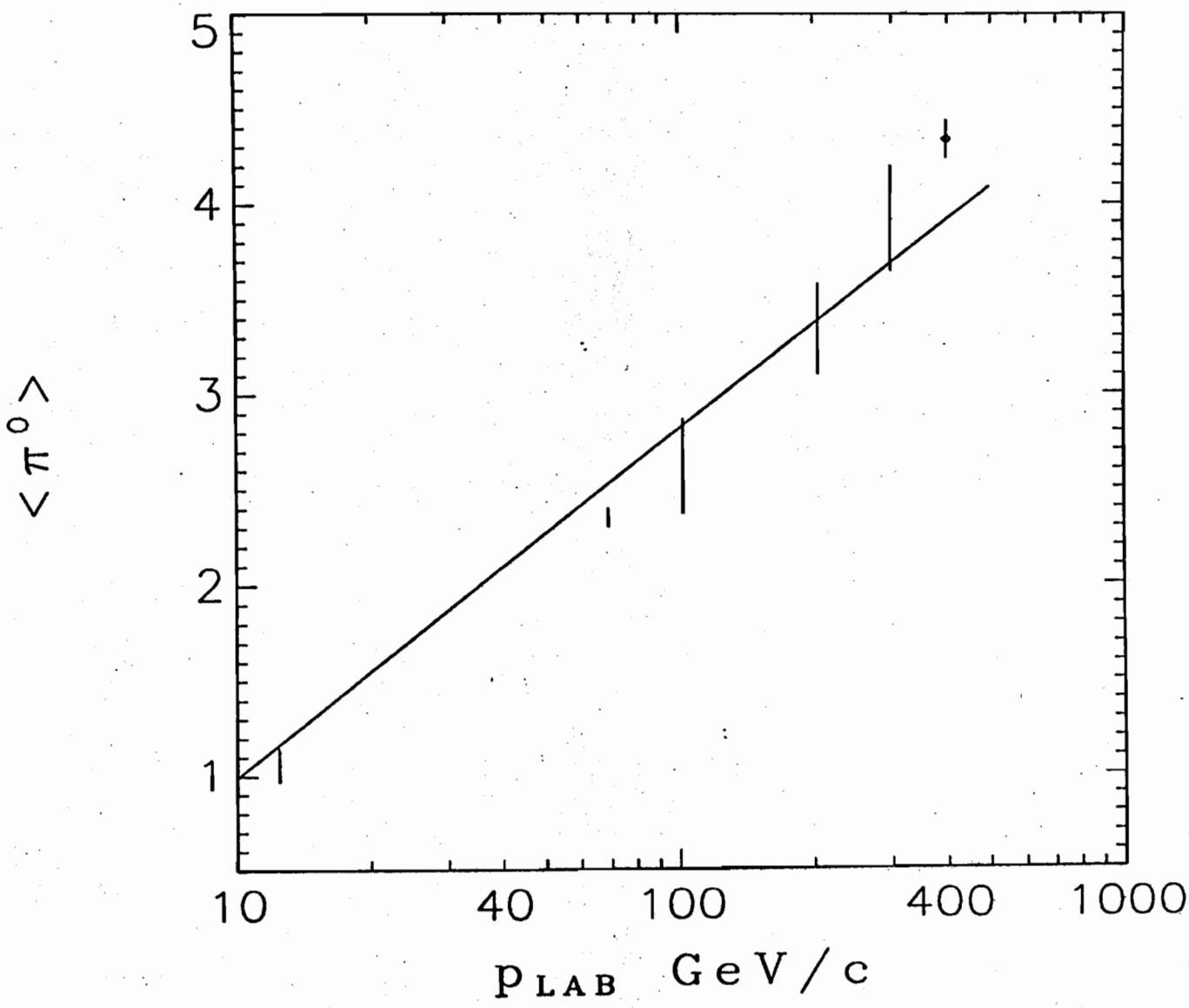

Figure 12

Average number of π^o's per inelastic collision as a function of incident laboratory momentum. The curve (Ref. 23) is a fit to previously existing data.

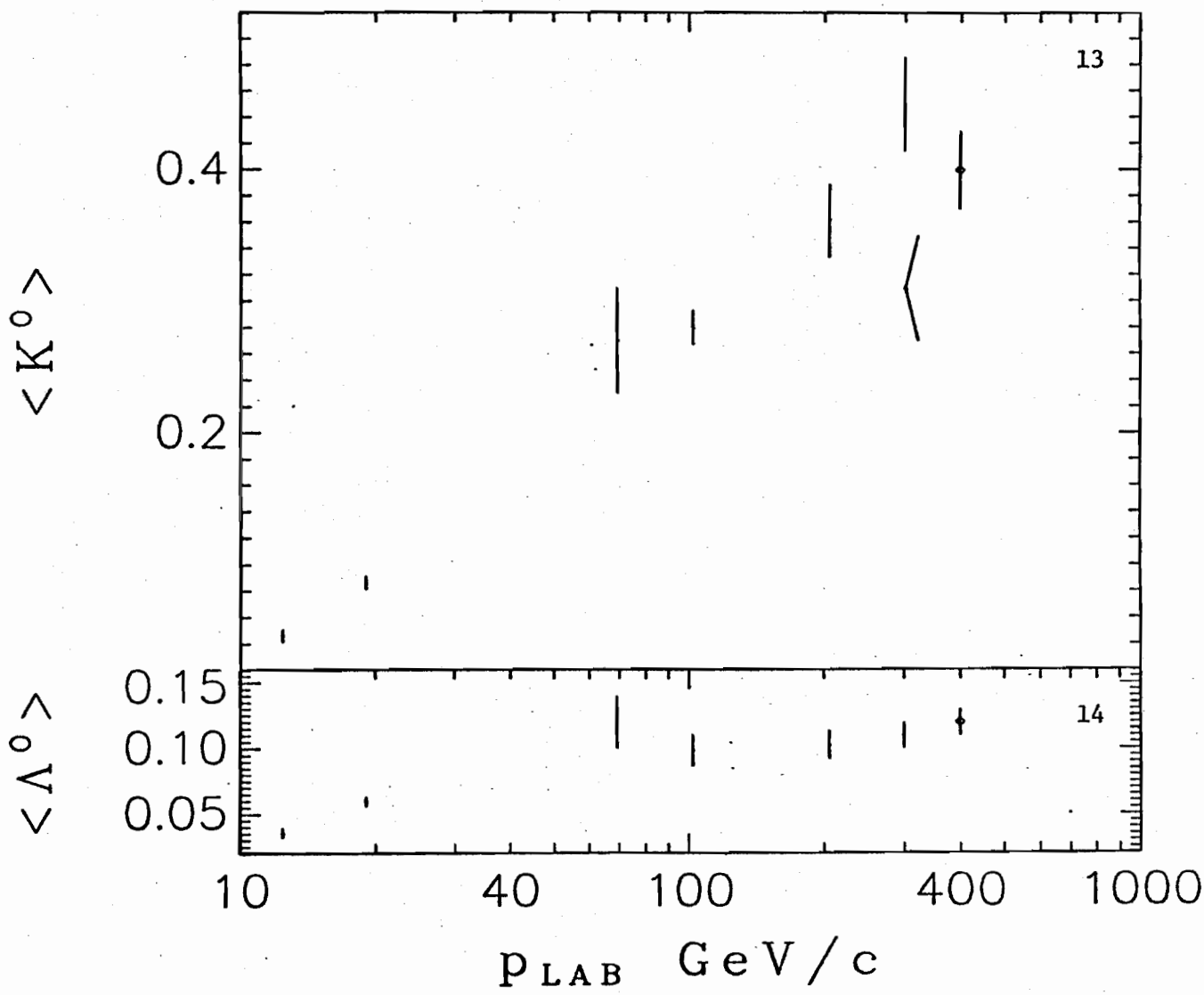

Figure 13: Average number of K^o's per inelastic collision as a function of incident laboratory momentum.

Figure 14: Average number of Λ^o's per inelastic collision as a function of incident laboratory momentum.

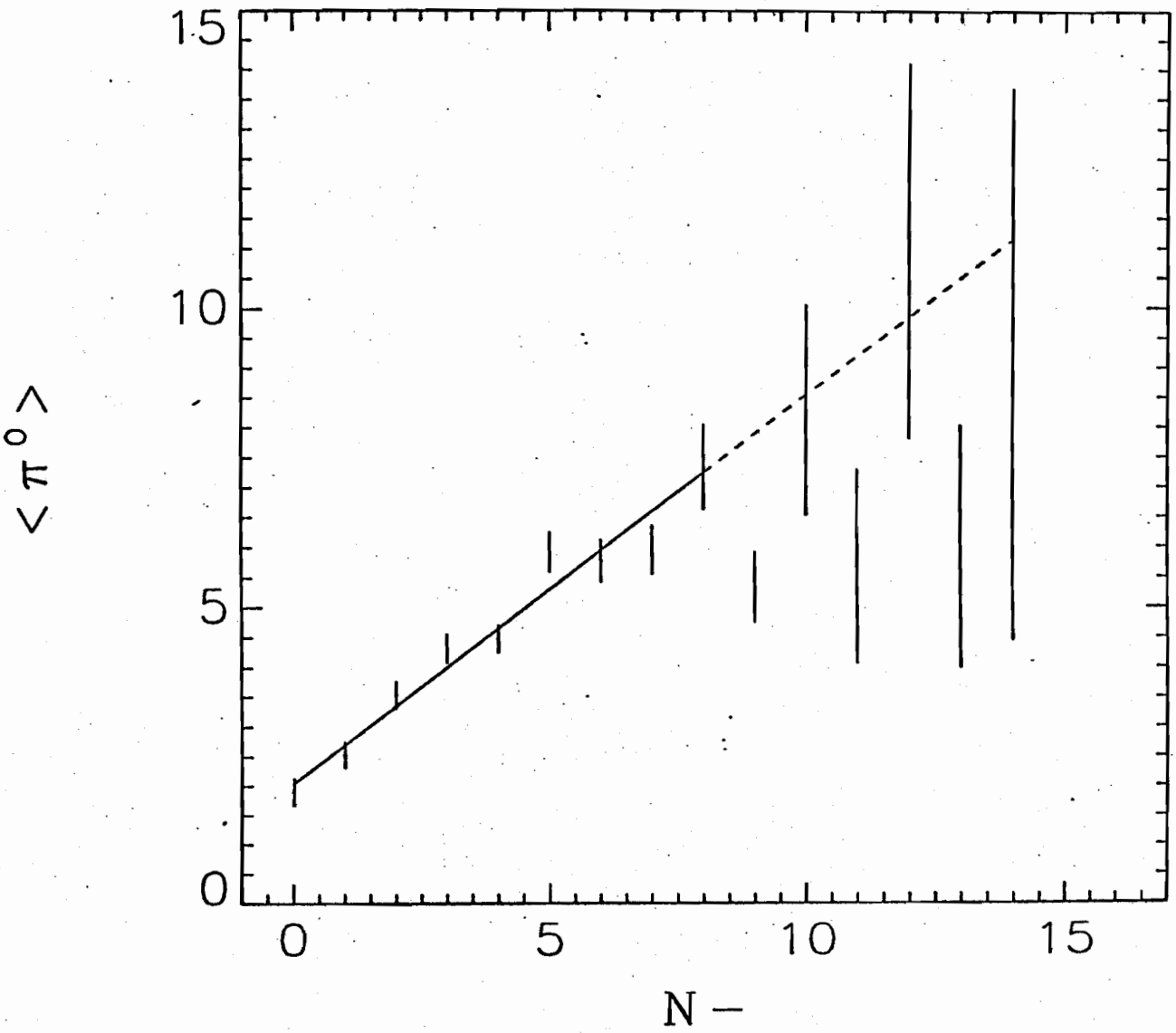

Figure 15

Average number of π^o's as a function of the number of negative particles (N_-) in an event. The solid line is a least squares fit to $\langle\pi^o\rangle = A + BN_-$ using the first points. The dashed curve is an extension of the solid curve.

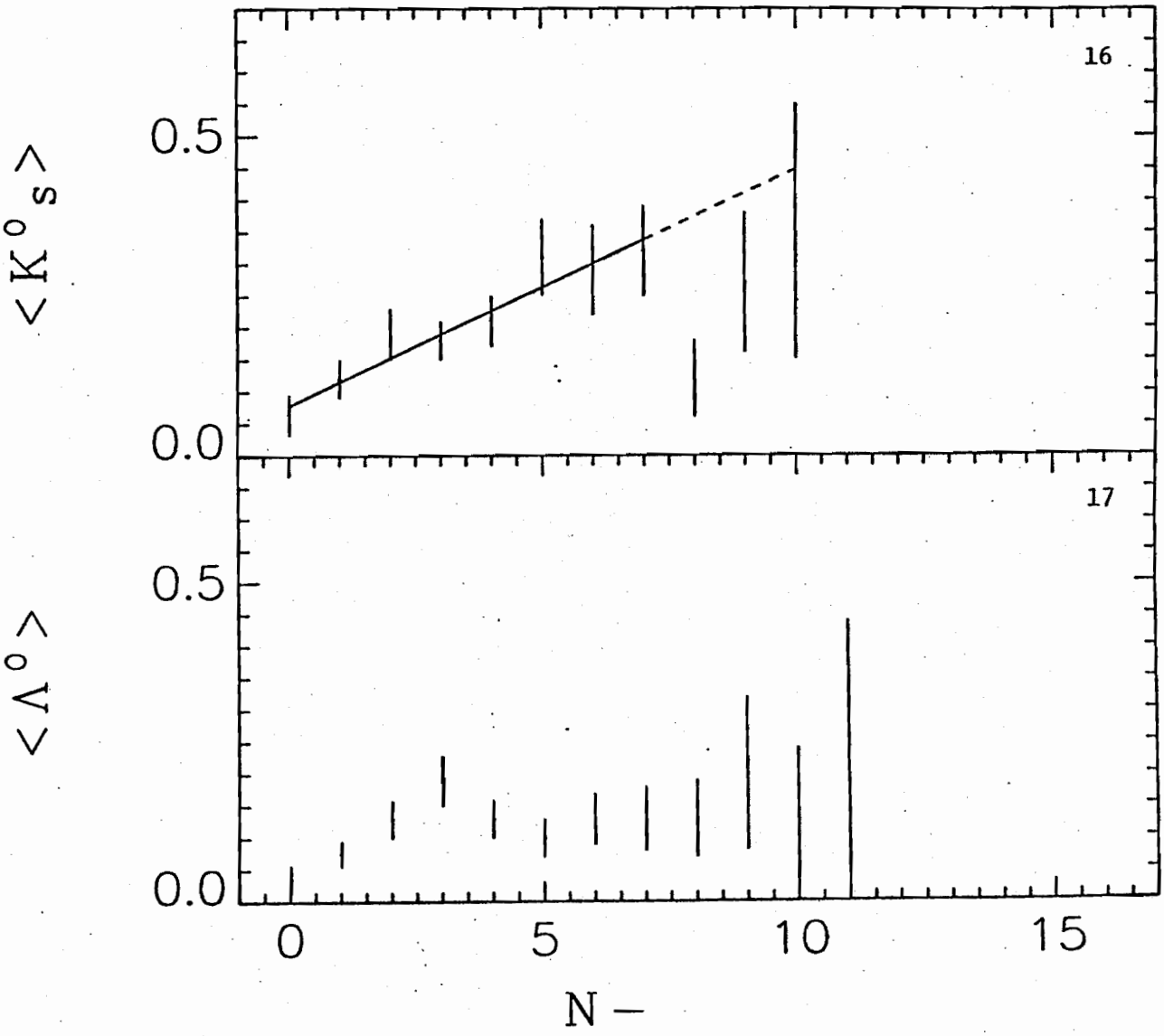

Figure 16: Average number of K^o_s's as a function of N_-. The solid curves are a least squares fit to $\langle K^o_s \rangle = A + BN_-$ using the first 8 points. The dashed curve is an extension of the solid curve.

Figure 17: Average number of Λ^o's as a function of N_-.

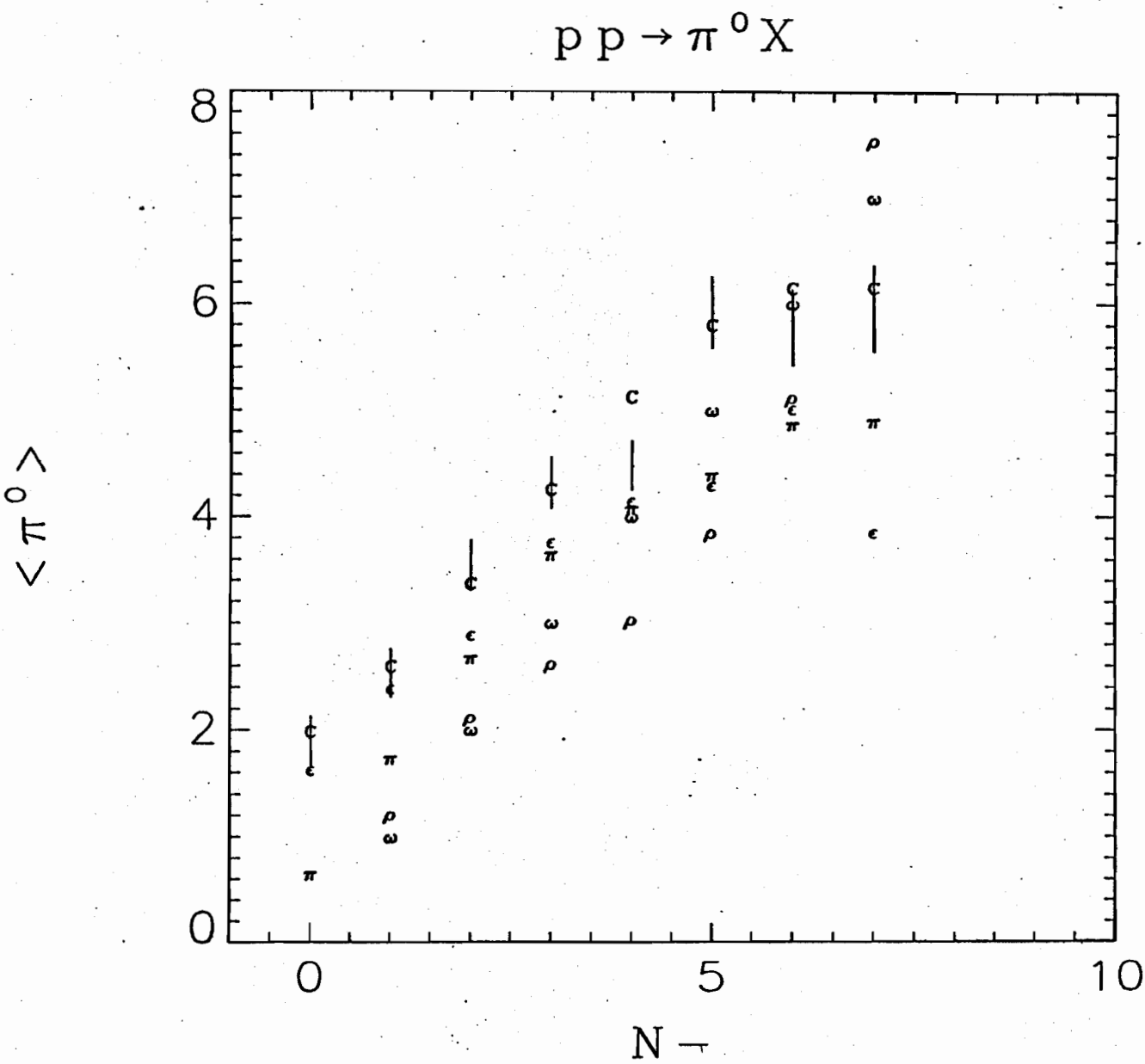

Figure 18

The predictions for the $\langle\pi^0\rangle$ vs N_- for the π, ε, ρ, ω, and Critical Fluid (C) model.

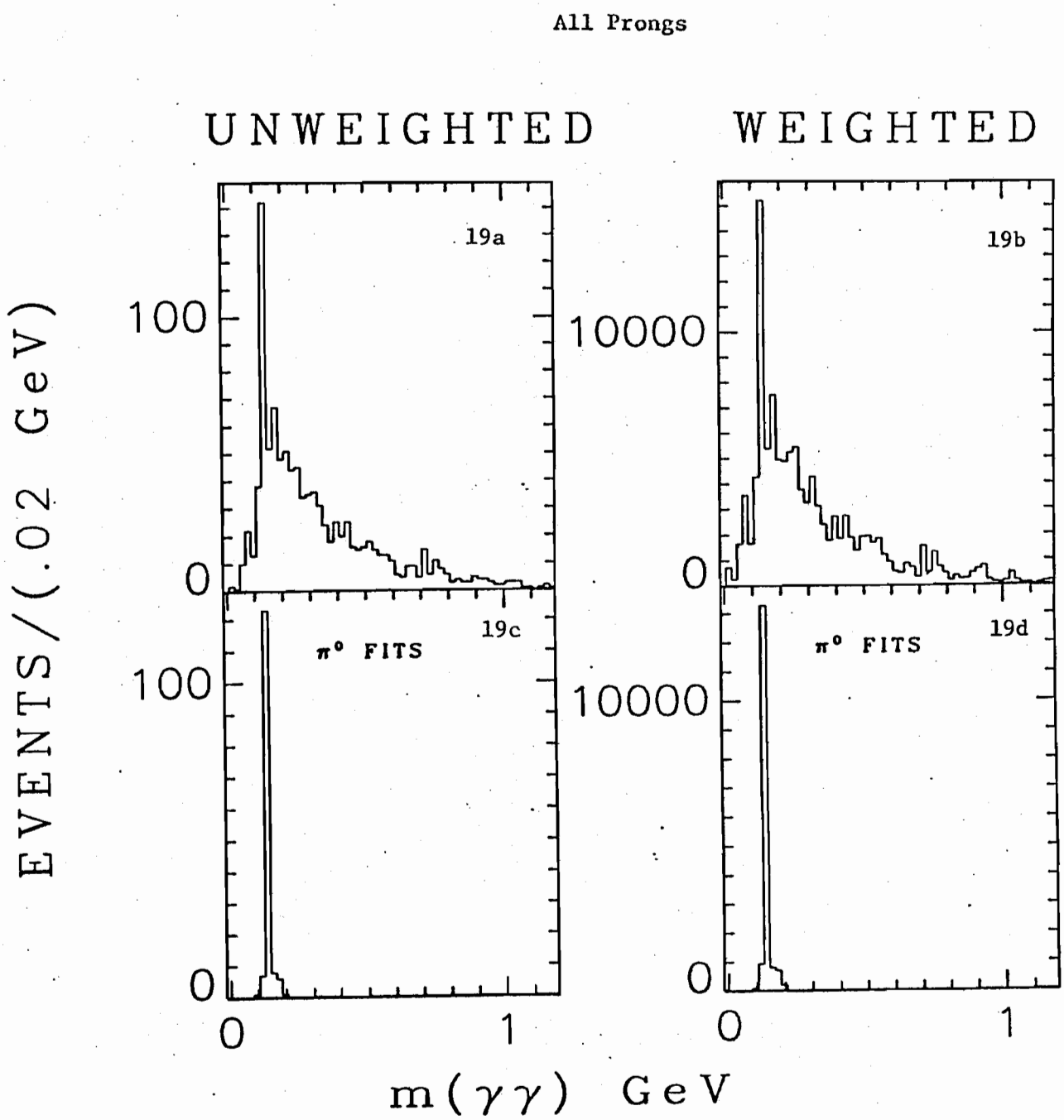

Figure 19a: Invariant mass distribution for γγ pairs.

Figure 19b: Weighted invariant mass distribution for γγ pairs.

Figure 19c: Events that fit (using SQUAW) π^o hypothesis.

Figure 19d: Weighted π^o fits.

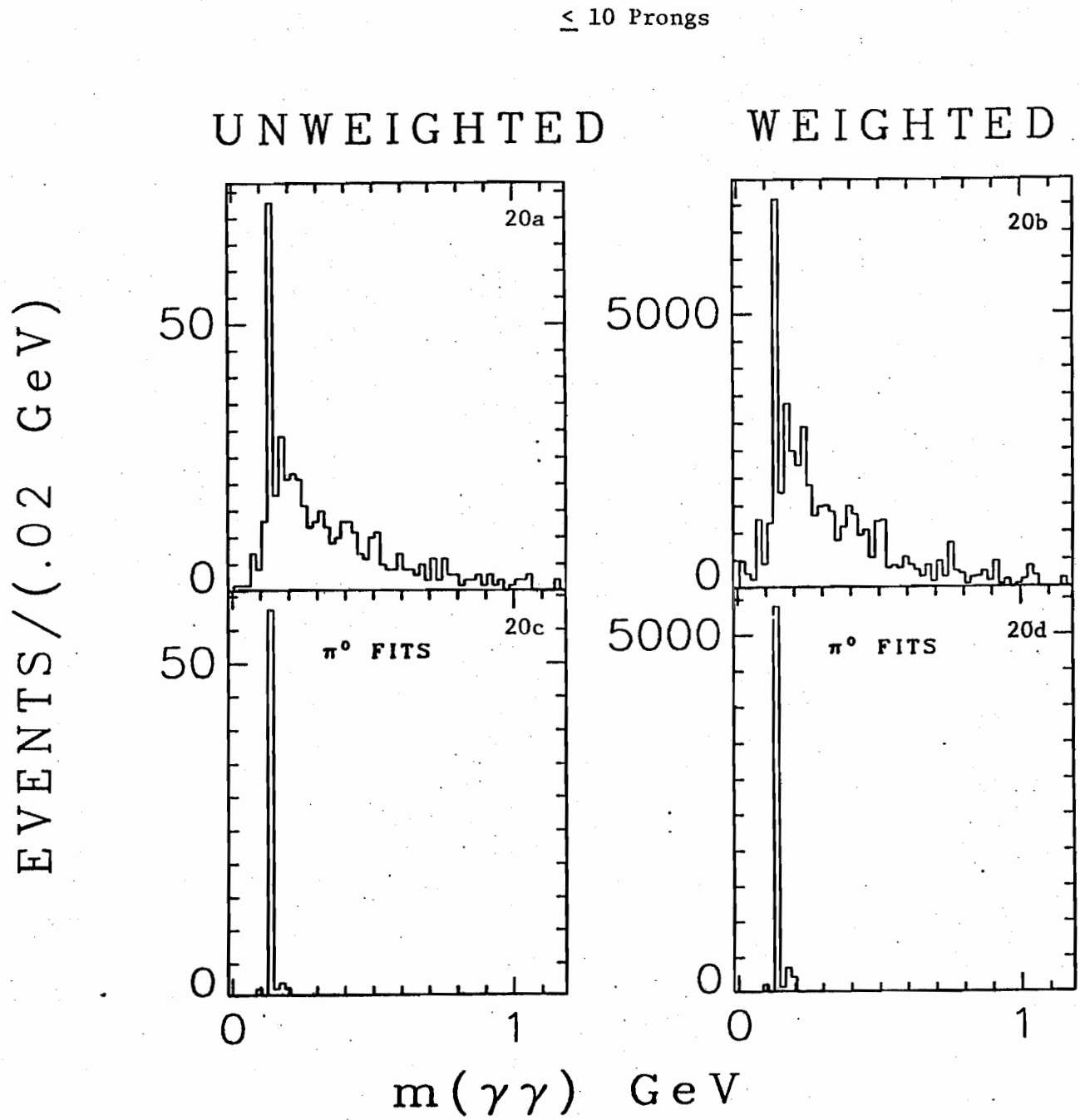

Figure 20a: Invariant mass distribution for γγ pairs.

Figure 20b: Weighted Invariant mass distribution for γγ pairs.

Figure 20c: Events that fit (using SQUAW) π^o hypothesis.

Figure 20d: Weighted π^o fits.

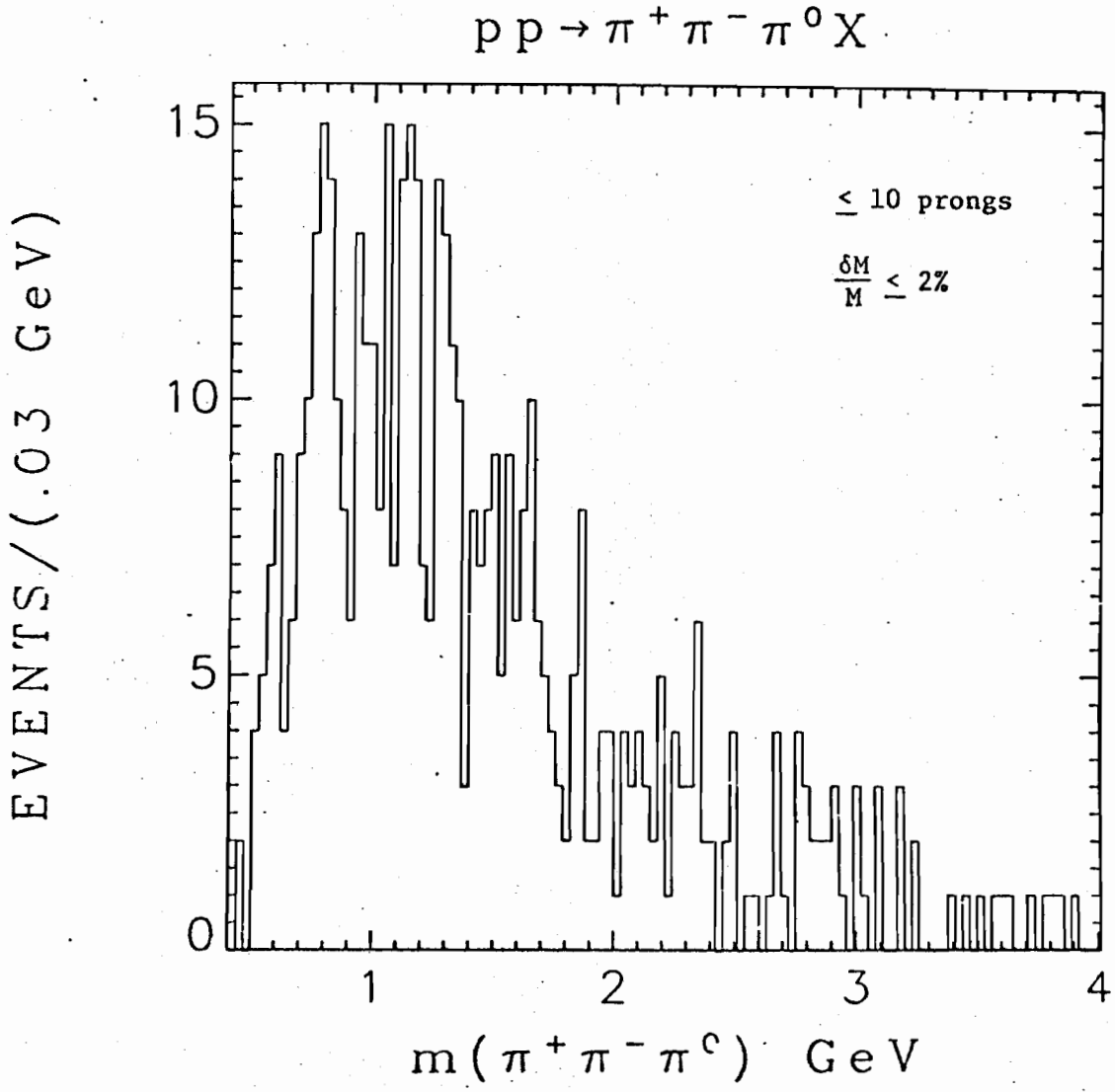

Figure 21

Invariant mass distribution for $\pi^+\pi^-\pi^0$ triplets.

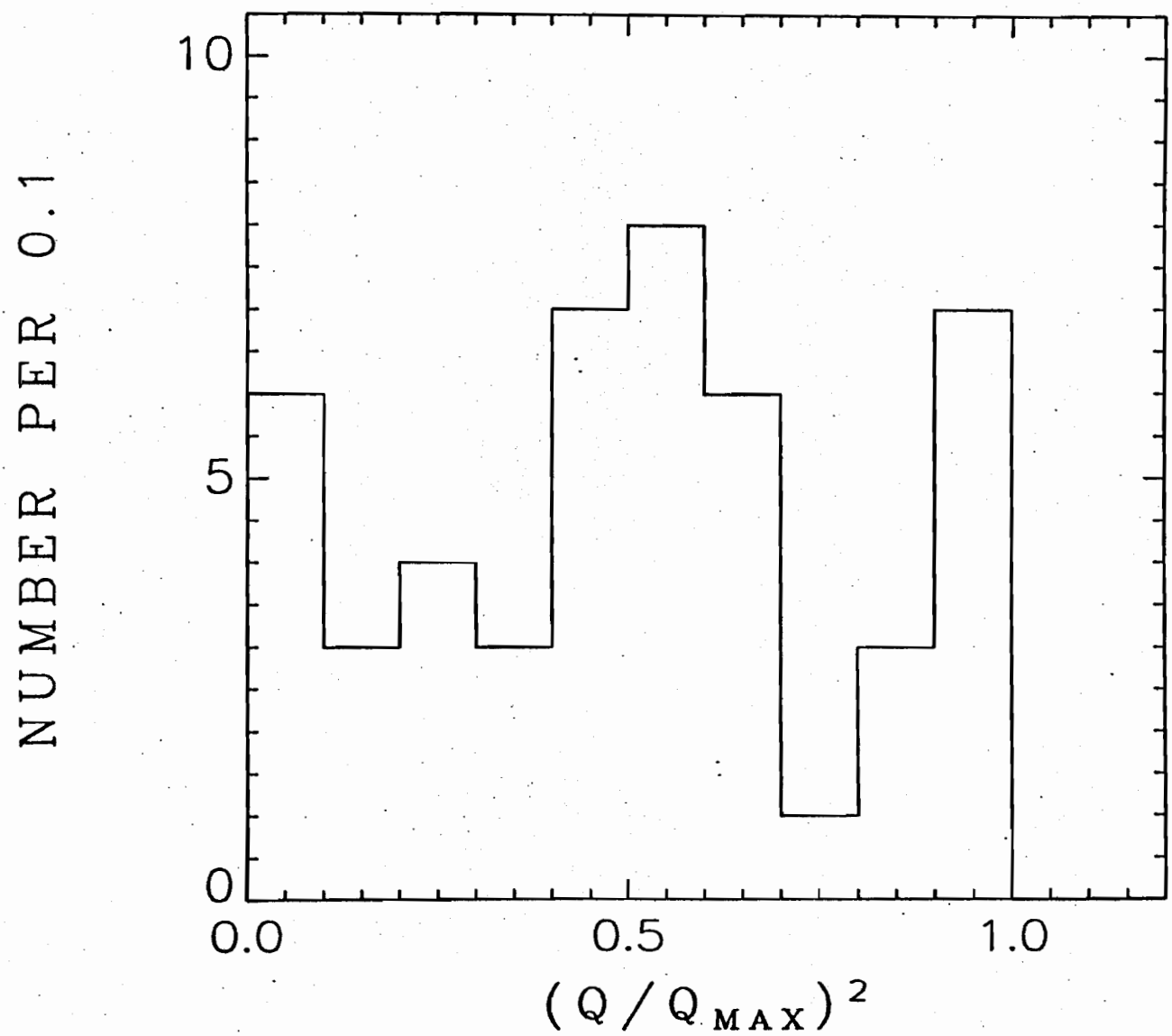

Figure 22

Distribution of $(Q/Q_{max})^2$.

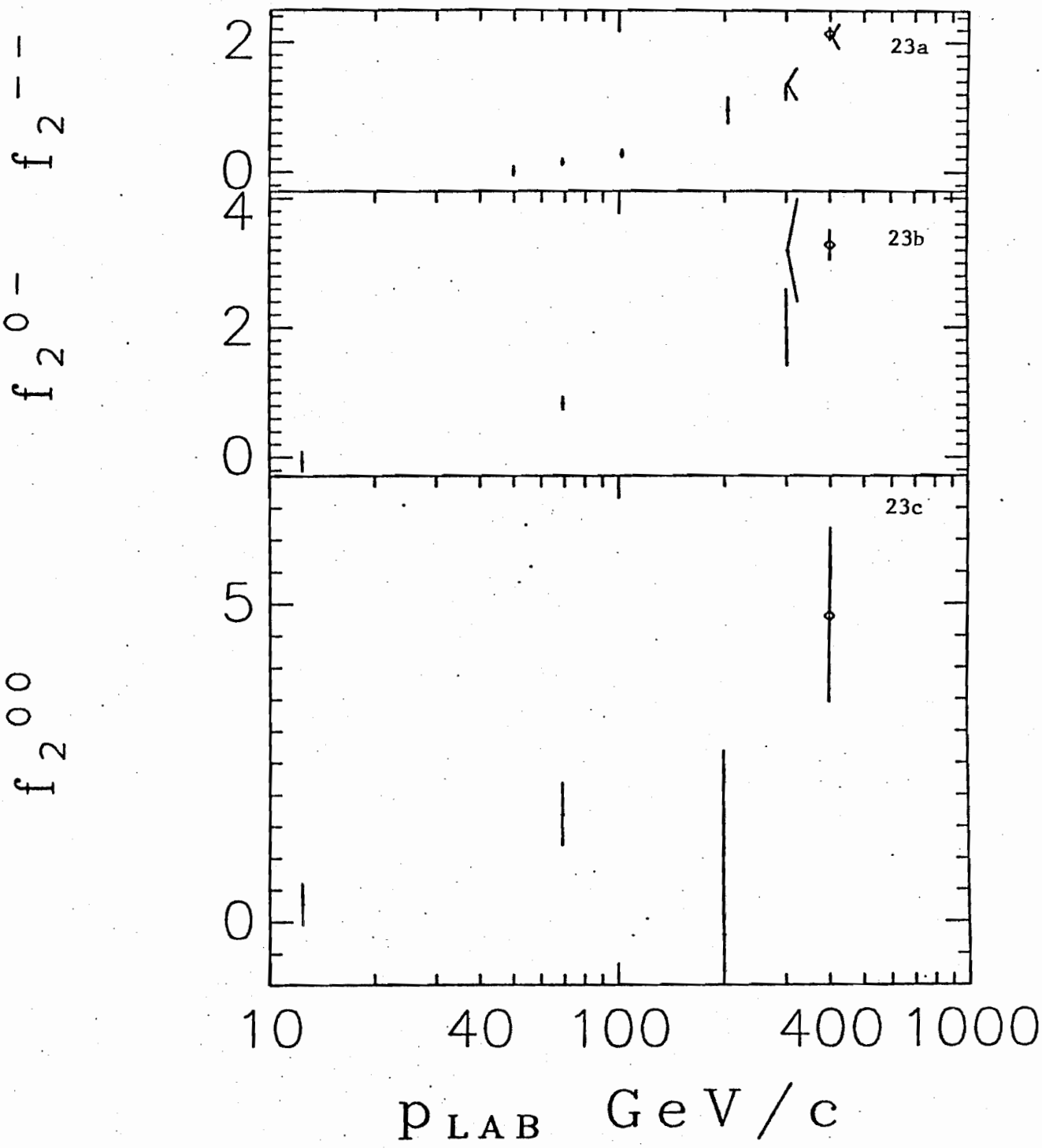

◇ = This experiment

Fig. 23a: f_2^{--} vs laboratory momentum.
Fig. 23b: f_2^{o-} vs laboratory momentum.
Fig. 23c: f_2^{oo} vs laboratory momentum.

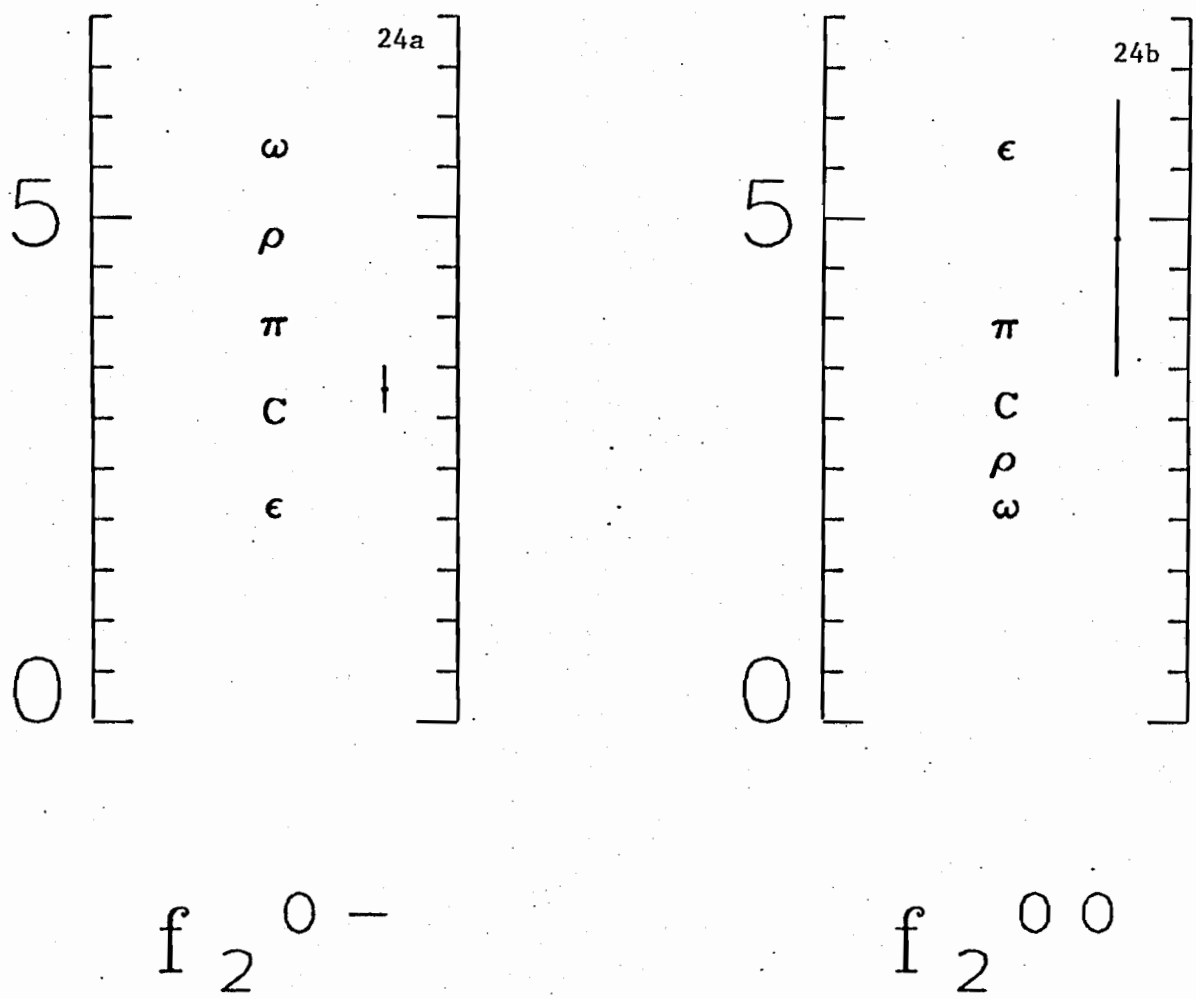

Figure 24a: Comparison of f_2^{0-} with predictions of ω, ρ, π, ε and Critical Fluid (C) model.

Figure 24b: Comparison of f_2^{00} with predictions of ω, ρ, π, ε and Critical Fluid (C) model.